1      Insights into particulate matter pollution in the North China Plain during wintertime:
2      Local contribution or regional transport?
3

4   Jiarui Wu[1,4], Naifang Bei[2], Yuan Wang[3], Xia Li[1,4], Suixin Liu[1,4], Lang Liu[1,4], Ruonan Wang[1,4], Jiaoyang
5   Yu[1], Min Zuo[1,4], Zhenxing Shen[2], Junji Cao[1,4], Xuexi Tie[1], and Guohui Li[1,4*]
6

7   [1]Key Lab of Aerosol Chemistry and Physics, SKLLQG, Institute of Earth Environment, Chinese Academy
8   of Sciences, Xi'an, 710061, China
9   [2]School of Human Settlements and Civil Engineering, Xi'an Jiaotong University, Xi'an, 710049, China
10   [3]Division of Geological and Planetary Sciences, California Institute of Technology, Pasadena, CA 91125,
11   USA
12   [4]CAS Center for Excellence in Quaternary Science and Global Change, Xi'an, 710061, China
13
14   [*]Correspondence to: Guohui Li (ligh@ieecas.cn)
15
16

17   **Abstract.** Accurate identification and quantitative source apportionment of fine particulate

18   matters ($PM_{2.5}$) provide an important prerequisite for design and implementation of emission

19   control strategies to reduce PM pollution. Therefore, a source-oriented version of the

20   WRF-Chem model is developed in the study to make source apportionment of $PM_{2.5}$ in the

21   North China Plain (NCP). A persistent and heavy haze event occurred in the NCP from 05

22   December 2015 to 04 January 2016 is simulated using the model as a case study to quantify

23   $PM_{2.5}$ contributions of local emissions and regional transport. Results show that local and

24   non-local emissions contribute 36.3% and 63.7% of the $PM_{2.5}$ mass in Beijing during the

25   haze event on average. When Beijing's air quality is excellent or good in terms of hourly

26   $PM_{2.5}$ concentrations, local emissions dominate the $PM_{2.5}$ mass with contributions exceeding

27   50%. However, when the air quality is severely polluted, the $PM_{2.5}$ contribution of non-local

28   emissions is around 75%. The non-local emissions also dominate the Tianjin's air quality,

29   with average $PM_{2.5}$ contributions exceeding 70%. The $PM_{2.5}$ level in Hebei and Shandong is

30   generally controlled by local emissions, but in Henan, local and non-local emissions play an

31   almost equivalent role in the $PM_{2.5}$ level, except when the air quality is severely polluted,

32   with non-local $PM_{2.5}$ contributions of over 60%. Additionally, the primary aerosol species are

33   generally dominated by local emissions with the average contribution exceeding 50%.

34   However, the source apportionment of secondary aerosols shows more evident regional

35   characteristics. Therefore, except cooperation with neighboring provinces to carry out strict

36   emission mitigation measures, reducing primary aerosols constitutes the priority to alleviate

37   PM pollution in the NCP, especially in Beijing and Tianjin.

38

39

## 1 Introduction

40

41    As the most polluted area in China, the North China Plain (NCP) has been suffering

42    severe particulate pollution for recent decades, particularly during wintertime, caused by a

43    synergy of local emissions, trans-boundary transport, specific topography, and unfavorable

44    meteorological situations (Long et al., 2016; Wu et al., 2017; An et al., 2019; Wu et al., 2020).

45    In recent years, China government has carried out aggressive emission mitigation measures to

46    reduce particulate matter (PM) pollution (Zheng et al., 2018; Zhang et al., 2019), but heavy

47    haze with high $PM_{2.5}$ (fine PM) concentrations still frequently engulfs the area. It is

48    controversial on whether local emissions or trans-boundary transport dominates the PM

49    pollution in the NCP, especially in Beijing (Guo et al., 2014; Li et al., 2015; Zhang et al., 2015;

50    Wu et al., 2017; Zamora et al., 2019). Therefore, accurate identification and quantitative

51    source apportionment (SA) of $PM_{2.5}$ are imperative to provide scientific reference for

52    instituting air quality control strategies as well as constitute an important prerequisite to

53    reduce PM pollution in the NCP.

54    The observation based SA techniques, such as chemical mass balance (CMB) and

55    positive matrix factorization (PMF) methods, are traditionally used to quantify the particle

56    contribution of each source (Cooper and Watson, 1980; Paatero and Tapper, 1993), but

57    cannot identify the source contribution of secondary transformation to particulate matters.

58    The brute force method (BFM) is the simplest model based SA method using air quality

59    models (AQMs) through zeroing out emissions from a specific source (Marmur et al., 2005).

60    The BFM can assess the importance of each emission source, but has flaws in quantifying the

61    source contribution due to lack of consideration of the complicated non-linear interaction

62    between various sources (Zhang and Ying, 2011). At present, the widely used SA technique

63    based on AQMs is the reactive tracer method or the source-oriented AQMs (Marmur et al.,

64    2006; Ying and Kleeman, 2006; Ying et al., 2008a; Ying et al., 2008b; Zhang and Ying, 2010,

65 2011; Burr and Zhang, 2011; Zhang et al., 2014). The method adds reactive tracers or tagged

66 species in AQMs to trace the atmospheric transport, transformation, and deposition of air

67 pollutants emitted from specific sources and quantify the source contribution according to the

68 mass conservation (Wagstrom et al., 2008; Wang et al., 2009).

69  The observation based SA method or the BFM based on AQMs has been used to

70 evaluate $PM_{2.5}$ contributions of local emissions and trans-boundary transport in the NCP,

71 especially in Beijing-Tianjin-Hebei (BTH). Chang et al. (2019) have investigated the

72 contribution of trans-boundary transport to the $PM_{2.5}$ concentration in 13 cities of the BTH,

73 showing that Shandong province has a considerable $PM_{2.5}$ contribution to most cities in BTH,

74 followed by Henan among the four neighboring provinces. Dong et al. (2020) have also

75 found that the regional transport contributes about 32.5%-68.4% of $PM_{2.5}$ concentrations in

76 BTH in 2017. However, the contribution of local emissions or trans-boundary transport to

77 Beijing's PM pollution still remains uncertain. Lang et al. (2013) have indicated that regional

78 transport accounts for 54.6% of $PM_{2.5}$ concentrations during the polluted episode in Beijing,

79 with annual $PM_{2.5}$ contribution of 42.4% on average using the observation and MM5–CMAQ

80 model results. Wu et al. (2017) have shown that non-Beijing emissions contribute 61.5% of

81 $PM_{2.5}$ mass during haze events in summer. However, some studies have emphasized that the

82 severe haze formation occurred in Beijing is mainly controlled by the efficient local aerosol

83 nucleation and growth, whereas the $PM_{2.5}$ contribution of regional transport might not be

84 significant (Guo et al., 2014; Zamora et al., 2019). Meng et al. (2020) found that the regional

85 transport from Hebei and Shandong plays an important role in the PM pollution in Tianjin,

86 with the average $PM_{2.5}$ contribution of 44% during the wintertime, but the local contribution

87 gradually dominates with continuous deterioration of the PM pollution. Wang et al. (2015)

88 have concluded that regional transport plays a non-negligible role in the top three polluted

89 cities in Hebei using the BFM method, with $PM_{2.5}$ contributions of 27.9% in Shijiazhuang,

90    46.6% in Xingtai, and 40.4% in Handan. However, Wang et al. (2019) have proposed that

91    local emissions are the main contributor to the air pollution in Hebei. Liu et al. (2017) have

92    emphasized that the contribution of regional transport to the PM pollution in Henan is

93    significant during the wintertime, with the average $PM_{2.5}$ contribution of 11.95%, 11.69%,

94    7.95%, and 7.4% from BTH, Anhui, Jiangsu, and Shandong, respectively. It is obvious that

95    whether local contribution or regional transport is dominant during the PM pollution in the

96    NCP is still uncertain.

97       In the study, a source-oriented WRF-Chem model is developed to comprehensively

98    quantify the contribution of local emissions and trans-boundary transport to the PM pollution

99    in the NCP, including Beijing, Tianjin, Hebei, Henan, and Shandong, as well as the adjacent

100    province on the west, Shanxi, under different pollution levels during the wintertime in 2015.

101

102    **2    Model and methodology**

103    **2.1    WRF-Chem model and configurations**

104       The source-oriented AQM used in the study is based on the WRF-Chem model (Version

105    3.5) (Grell et al., 2005) with modifications by Li et al. (2010, 2011a, 2011b). The modified

106    WRF-Chem model includes a new flexible gas phase chemical module that can be used with

107    different chemical mechanisms and the CMAQ aerosol module (AERO5) developed by US

108    EPA (Binkowski and Roselle, 2003; Foley et al., 2010). The wet deposition is based on the

109    method in the CMAQ module and the dry deposition of chemical species follows Wesely

110    (1989). The photolysis rates are calculated using the Fast Tropospheric Ultraviolet and

111    Visible (FTUV) Radiation Model with the aerosol and cloud effects on photolysis (Li et al.,

112    2005; Li et al., 2011a). The inorganic aerosols are predicted using ISORROPIA Version 1.7,

113    calculating the composition and phase state of an ammonium-sulfate-nitrate-water inorganic

114    aerosol in thermodynamic equilibrium with gas phase precursors (Nenes et al., 1998). The

Atmospheric
Chemistry
and Physics
Discussions

115    secondary organic aerosols (SOA) are calculated using the volatility basis-set (VBS)

116    modeling method, with contributions from glyoxal and methylglyoxal. Detailed information

117    can be found in Li et al. (2010, 2011a, 2011b). Figure 1 shows the simulation domain and

118    detailed model configuration can be found in Table 1.

119    **2.2  Source-Oriented WRF-Chem model**

120    In the source-oriented WRF-Chem model, the SAPRC-99 photochemistry mechanism

121    (Carter, 2010) and CMAQ aerosol module (AERO5) (Foley et al., 2010) are modified so that

122    the precursors of aerosols from different sources and their corresponding reaction products

123    are treated as different species and tracked independently in chemical, physical, and dynamic

124    processes. It is worth noting that the tagged species have exactly identical physical and

125    chemical properties as the original ones.

126    Black carbon and unspecified species (mainly mineral dust) from each source are tagged

127    and only tracked in processes of transport, dispersion, and wet/dry deposition since they do

128    not involve in photochemistry and gas-to-particle partitioning. For the inorganic aerosols

129    (sulfate, nitrate, and ammonium) and organic aerosols (primary and secondary organic

130    aerosols, i.e., POA and SOA), their precursors from each source and corresponding reaction

131    products are treated as different species and simulated in the SAPRC-99 photochemistry

132    mechanism and traced in processes of transport, dispersion, and wet/dry deposition as well as

133    gas-to-particle partitioning. A non-hardwired gas phase chemical module is used to solve the

134    SAPRC-99 photochemistry based on the Eulerian backward Gauss-Seidel iterative technique

135    (Hess et al., 2000; Li et al., 2010). The module is flexible to include a new gas-phase species

136    and its corresponding photochemical reactions.

137    The ISORROPIA is used to distribute the $NH_3$/ammonium, $HNO_3$/nitrate, and water

138    between the gas and aerosol phases as a function of total sulfate, total ammonia, total nitrate,

139    relative humidity and temperature (Nenes et al., 1998). Therefore, as a bulk method, the

140   ISORROPIA cannot be applied to distribute the gas and aerosol phase for the inorganic

141   aerosol from each source separately because of the interaction among various sources.

142     Except primary emissions, the SA for sulfate aerosols needs to be considered in the

143   homogenous and heterogeneous formation pathways. The sulfate growth from the gas-phase

144   $SO_2$ oxidation is contributed by the $H_2SO_4$ involved nucleation and condensation, which are

145   determined by the $H_2SO_4$ formation rate in the atmosphere. At time $(t)$, after one time step

146   $(\delta t)$ integeration, the conceptual scheme of the source-oriented sulfate gas-phase formation is

147   shown in Figure 2a. In the study, the heterogeneous conversion of $SO_2$ is parameterized as

148   the $SO_2$ oxidation involving aerosol water by $O_2$ catalyzed by $Fe^{3+}$. Figure 2b presents the

149   sulfate SA for the heterogeneous formation. The SA for nitrate and ammonium aerosols

150   follows the mass conversion of $N(+VI)$ and $N(-III)$ from each source, respectively,

151   when the total ammonia and nitrate are distributed between the gas and aerosol phases by the

152   ISORROPIA after one time step integration, as shown in Figure 3.

153     Organic aerosols are simulated using a non-traditional SOA module based on the

154   volatility basis set (VBS) method, in which all primary species are treated as chemically

155   reactive and distributed in logarithmically spaced volatility bins (Donahue et al., 2006;

156   Robinson et al., 2007). Nine surrogate species with saturation concentration ranging from

157   $10^{-2}$ to $10^6$ μg m$^{-3}$ at room temperature are considered to represent POA compositions

158   (Shrivastava et al., 2008). The SOA formation from anthropogenic or biogenic precursors is

159   predicted using four semi-volatile organic compounds (SVOCs) whose effective saturation

160   concentrations at room temperature are 1, 10, 100, and 1000 μg m$^{-3}$, respectively (Tsimpidi et

161   al., 2010). The SOA formation includes the following pathways: (1) the oxidation of VOCs

162   emitted from anthropogenic and biogenic sources, (2) intermediate VOCs (IVOCs)

163   co-emitted with POA but are never in the particle phase during the emissions process

164   oxidized by OH, and (3) primary organic gases (POG) emitted or formed due to evaporation

Atmospheric
Chemistry
and Physics
Discussions
Open Access
EGU

165   of POA assumed to react with OH radicals to reduce their volatility and hence to partition

166   between gas and particle phase forming SOA (Odum et al., 1996; Pankow, 1994; Lipsky and

167   Robinson, 2006; Robinson et al., 2007; Shrivastava et al., 2006). The VBS method is in

168   principle source-oriented, which can be used to trace the OA formation from various sources.

169   Therefore, when considering SA for organic aerosols, we just need to treat all the SOA and

170   POA as well as their corresponding gas-phase organics from each emission source as the

171   VBS input, as shown in Figure 4a. For the heterogeneous pathway, the SOA formation from

172   glyoxal and methyglyoxal is parameterized as a first-order irreversible uptake on aerosol or

173   cloud droplet surfaces with a reactive uptake coefficient of $3.7 \times 10^{-3}$ (Volkamer et al., 2007;

174   Zhao et al., 2006). The SA for heterogeneous SOA formation is shown in Figure 4b, which is

175   similar to that for heterogeneous sulfate formation.

176   **2.3   Data and statistical methods for comparisons**

177   The model performance in simulating $PM_{2.5}$, $O_3$, $NO_2$, $SO_2$, and CO is validated using

178   the hourly observations released by Ministry of Ecology and Environment of China (China

179   MEP). In addition, the predicted submicron sulfate, nitrate, ammonium, and organic aerosols

180   are compared to measurements by the Aerodyne Aerosol Chemical Speciation Monitor

181   (ACSM), which is deployed at the National Center for Nanoscience and Technology

182   (NCNST), Chinese Academy of Sciences in Beijing (Figure 1). The primary organic aerosol

183   (POA) and SOA concentrations are obtained from the ACSM measurement analyzed using

184   the positive matrix factorization (PMF).

185   In the present study, the mean bias (*MB*), root mean square error (*RMSE*) and the index

186   of agreement (*IOA*) are used as indicators to evaluate the performance of WRF-Chem model.

187   *IOA* describes the relative difference between the model and observation, ranging from 0 to 1,

188   with 1 indicating perfect agreement.

189   $$MB = \frac{1}{N}\sum_{i=1}^{N}(P_i - O_i)$$

190 $$RMSE = \left[\frac{1}{N}\sum_{i=1}^{N}(P_i - O_i)^2\right]^{\frac{1}{2}}$$

191 $$IOA = 1 - \frac{\sum_{i=1}^{N}(P_i - O_i)^2}{\sum_{i=1}^{N}(|P_i - \overline{O}| + |O_i - \overline{O}|)^2}$$

192 Where $P_i$ and $O_i$ are the predicted and observed pollutant concentrations, respectively. $N$ is

193 the total number of the predictions used for comparisons, and $\overline{P}$ and $\overline{O}$ represents the

194 average of the prediction and observation, respectively.

195

196 **3    Results and discussions**

197 **3.1  Model performance**

198    Figure 5 shows the diurnal profiles of observed and simulated near-surface $PM_{2.5}$, $O_3$,

199 $NO_2$, $SO_2$ and CO concentrations averaged at monitoring sites in the NCP from 05 December

200 2015 to 04 January 2016. The model generally performs well in reproducing the temporal

201 variation of $PM_{2.5}$ concentrations in the NCP, with an $IOA$ of 0.96, but slightly overestimates

202 $PM_{2.5}$ concentrations against measurements, with a $MB$ of 2.2 μg m$^{-3}$. The diurnal $O_3$

203 variation is successfully replicated by the model, such as peak afternoon $O_3$ concentrations

204 caused by active photochemistry and low nighttime $O_3$ concentrations due to the $NO_x$ titration,

205 with an $IOA$ of 0.88. However, the model is subject to underestimating the $O_3$ concentration

206 compared to measurements, particularly during nighttime, with a $MB$ of -5.9 μg m$^{-3}$. The

207 model also reasonably well reproduces the $NO_2$ diurnal profiles with peaks in the evening,

208 with an $IOA$ of 0.89 and a $MB$ of 0.5 μg m$^{-3}$, but considerable overestimations or

209 underestimations still exist. The model generally tracks reasonably the temporal variation of

210 $SO_2$ concentrations against observations, with an $IOA$ of 0.76. However, the biases for the

211 $SO_2$ simulation are also large considering that $SO_2$ is mainly emitted from point sources and

212 its simulations are more sensitive to the wind field uncertainties (Bei et al., 2017). Compared

213 with measurements, the temporal profile of the near-surface CO concentration in the NCP is

214  well simulated, with the *IOA* and *MB* of 0.90 and 0.0 µg m$^{-3}$, respectively.

215      Figure 6 shows the spatial pattern of simulated and observed average near-surface

216  concentrations of $PM_{2.5}$, $O_3$, $NO_2$, and $SO_2$ along with simulated winds during the episode in

217  the NCP. The simulated air pollutants distributions are generally in good agreement with

218  observations, although the model biases still exist. During the haze episode, the simulated

219  weak or calm winds are favorable for accumulation of air pollutants, leading to formation of

220  the serious air pollution in the NCP. The simulated average near-surface $PM_{2.5}$ concentrations

221  during the episode are more than 115 µg m$^{-3}$ in the NCP, which is consistent with

222  observations. The simulated and observed average $O_3$ concentrations during the episode are

223  not high, generally less than 40 µg m$^{-3}$. The low $O_3$ concentration during the episode is

224  chiefly caused by the slow photochemical activities due to weak wintertime insolation which

225  is further attenuated by clouds and aerosols and the resultant titration of high $NO_x$ emissions

226  (Li et al., 2018). The observed and calculated average $NO_2$ and $SO_2$ concentrations are still

227  high in the NCP, varying from 30 to 100 µg m$^{-3}$ and 20 to 100 µg m$^{-3}$, respectively, although

228  strict emission mitigation measures have been carried out since 2013. Interestingly, the

229  simulated $SO_2$ concentrations in cities and their surrounding areas are very high, but the

230  simulated $NO_2$ concentrations present uniform distribution in the NCP, indicating the

231  substantial contribution of $NO_x$ area sources.

232      Figure 7 provides the temporal variations of simulated and observed aerosol species at

233  NCNST in Beijing during the episode. Generally, the model predicts reasonably the temporal

234  variations of the aerosol species against the measurements. The model yields the major peaks

235  of the POA concentration compared to observations in Beijing, but frequently underestimates

236  or overestimates the POA concentration, with an *IOA* of 0.80 and a *MB* of -2.0 µg m$^{-3}$. As a

237  primary species, the POA in Beijing is determined by local emissions and regional transport

238  outside of Beijing during haze days, so uncertainties from emissions and meteorological

Atmospheric
Chemistry
and Physics
Discussions

Open Access

EGU

239    fields have large potential to influence POA simulations (Bei et al., 2017). Although the VBS

240    modeling method is used and contributions from glyoxal and methylglyoxal are included in

241    the study, the model still has difficulties in simulating the SOA concentrations, with the *IOA*

242    and *MB* of 0.67 and -10.5 $\mu g\ m^{-3}$, respectively. Except the SOA formation and transformation

243    mechanism in the atmosphere, which remains elusive, many factors have potentials to affect

244    the SOA simulation, such as meteorology, measurements, precursor emissions, and SOA

245    treatments (Li et al., 2011). The model reasonably reproduces the sulfate temporal variation

246    compared to measurements, and the *MB* and *IOA* are -3.5 $\mu g\ m^{-3}$ and 0.87, respectively. The

247    model also performs well in simulating the nitrate and ammonium concentrations against

248    measurements in Beijing, with *IOAs* of 0.92 and 0.88, respectively.

249        Generally, the model simulates well the spatial distribution and temporal variation of air

250    pollutants in the NCP, and the predicted aerosol species are also consistent well with the

251    measurements in Beijing. Good model performance in simulating air pollutants and aerosol

252    species provides a reliable base for quantifying contributions of local and non-local emissions

253    to the PM pollution in the NCP.

254    **3.2  Source apportionment of the PM pollution in the NCP**

255        We have marked the emitted precursors in six provinces, including Beijing, Tianjin,

256    Hebei, Henan, Shandong, and Shanxi in simulations of the source-oriented WRF-Chem

257    model (Figure 1). Additionally, the boundary transport and emissions from the region except

258    the six provinces are taken as the background source. Therefore, $PM_{2.5}$ contributions of the

259    non-local emission for each of the six provinces include those transported from the other five

260    provinces and the background source.

261        Figure 8 shows the average $PM_{2.5}$ contribution of emissions from the six provinces

262    during the study episode. Apparently, emissions from the six provinces influence the $PM_{2.5}$

263    level in the whole NCP, showing necessity of collaborative emission mitigation to reduce PM

**264** pollution. Emissions of Hebei, Henan, and Shandong not only significantly deteriorate the

**265** local PM pollution, with $PM_{2.5}$ contributions ranging from 50 to over 100 μg m$^{-3}$, also

**266** considerably enhance the $PM_{2.5}$ level in their surrounding areas by about 5~50 μg m$^{-3}$.

**267** Emissions of Beijing and Tianjin increase the local $PM_{2.5}$ concentrations by 10~100 μg m$^{-3}$,

**268** and contribute about 3~10 μg m$^{-3}$ $PM_{2.5}$ to their surrounding areas. Due to blocking of

**269** mountains, $PM_{2.5}$ contributions of the Shanxi emission to the NCP is not significant, ranging

**270** from 3 to 20 μg m$^{-3}$.

**271** Beijing is surrounded from the southwest to the northeast by the Taihang Mountains and

**272** the Yanshan Mountains and open to the NCP in the south and east. During haze events,

**273** southerly or easterly winds are generally prevailed in the NCP, facilitating transport of air

**274** pollutants emitted from the NCP to Beijing and further accumulation due to the mountain

**275** blocking (Long et al., 2016). During the study episode, the average simulated $PM_{2.5}$

**276** concentration in Beijing is around 125.3 μg m$^{-3}$, in which the contribution of local emissions

**277** is 36.3%. The remaining 63.7% of $PM_{2.5}$ concentrations in Beijing is accounted for by

**278** non-Beijing emissions, showing that Beijing's air quality is dominated by non-Beijing

**279** emissions during the PM pollution episode. The $PM_{2.5}$ contribution of Hebei emissions to

**280** Beijing is 24.6%, greater than those of Shandong (8.3%), Tianjin (7.4%), Henan (3.6%), and

**281** Shanxi (3.3%). The background source contributes about 16.5% of the $PM_{2.5}$ mass in Beijing

**282** on average. Overall, the contribution of emissions from Beijing's five surrounding provinces

**283** to the $PM_{2.5}$ mass is 47.2%, exceeding that of local emissions, indicating the importance of

**284** the trans-boundary transport of air pollutants in the haze formation in Beijing. Adjacent to

**285** Beijing, the Tianjin's air quality is also dominated by trans-boundary transport of air

**286** pollutants. The average $PM_{2.5}$ contribution of non-local emissions is 76.2%, in which Hebei,

**287** Shandong, Beijing, Henan, and Shanxi accounts for 29.3%, 11.7%, 8.0%, 4.0%, and 3.0%,

**288** respectively. The $PM_{2.5}$ contribution of local emissions in Hebei, Henan, and Shanxi is

Atmospheric
Chemistry
and Physics
Discussions
EGU
Open Access

289 almost as much as that of trans-boundary transport, with the average of 50.2%, 45.7%, and

290 49.2%, respectively. The Shandong emissions play an important role in the air quality in

291 Hebei and Henan, with $PM_{2.5}$ contributions of about 15%. Moreover, the Shandong's air

292 quality is primarily determined by emissions of itself, with an average $PM_{2.5}$ contribution of

293 64.9%. Emissions of Beijing, Tianjin, Hebei, Henan, and Shanxi contribute less than 8% of

294 the $PM_{2.5}$ mass in Shandong. The background source makes up approximately 20.1%, 11.4%,

295 16.8%, 11.4%, and 21.8% of the $PM_{2.5}$ mass in Tianjin, Hebei, Henan, Shandong, and Shanxi,

296 respectively.

297 Previous studies have shown that there exist large uncertainties on the contribution of

298 local emissions or trans-boundary transport to Beijing's PM pollution (Guo et al., 2010; Guo

299 et al., 2014; Li et al., 2015; Zhang et al., 2015; Wu et al., 2017). We further evaluate the

300 contribution of local and non-local emissions to the $PM_{2.5}$ mass in Beijing under different

301 pollution levels, as well as in the other five provinces. The simulated hourly near-surface

302 $PM_{2.5}$ mass concentrations in Beijing during the whole episode are first subdivided into 6

303 bins based on the air quality standard in China for $PM_{2.5}$, i.e., 0~35 (excellent), 35~75 (good),

304 75~115 (lightly polluted), 115~150 (moderately polluted), 150~250 (heavily polluted), and

305 exceeding 250 (severely polluted) $\mu g\ m^{-3}$ (Feng et al., 2016). $PM_{2.5}$ contributions from local

306 emissions and the other five provinces as well as background source to Beijing are assembled

307 separately as the bin $PM_{2.5}$ concentrations following the grid cells, and an average of $PM_{2.5}$

308 contributions from each source in each bin is calculated. The same method is also used for

309 the other five provinces.

310 Table 2, Table 3 and Figure 9 present the average percentage contribution of local and

311 non-local emissions to the $PM_{2.5}$ concentrations in Beijing, Tianjin, Hebei, Henan, Shandong,

312 and Shanxi during the episode under different pollution levels. The local emission dominates

313 the $PM_{2.5}$ mass when the air quality is excellent and good in Beijing, with the average

314  contribution of 56.8% and 55.0%, respectively. Moreover, the $PM_{2.5}$ contribution of local

315  emissions decreases with the deterioration of the air quality in Beijing, with an average

316  contribution of 48.7%, 40.5%, 35.4%, and 25.1%, respectively, when the air quality is

317  slightly, moderately, heavily, and severely polluted. Therefore, non-local emissions play a

318  dominant role in Beijing's PM pollution, particularly when the air quality is severely polluted,

319  non-local emissions contribute around 75% of the $PM_{2.5}$ mass in Beijing. With the excellent

320  and good air quality in Beijing, the contribution of emissions from the other five provinces is

321  22.4% and 29.5%, respectively, much less than those of local emissions. However, the

322  contribution increases from 37.6% to 54.3% with deterioration of Beijing's air quality from

323  being slightly to severely polluted. The result is consistent with that from Lang et al. (2013),

324  reporting that regional transport accounts for 54.6% of the $PM_{2.5}$ mass in Beijing during a PM

325  pollution episode. Additionally, Jiang et al. (2015) have concluded that the transport from the

326  environs of Beijing contributes about 55% of the peak $PM_{2.5}$ concentration in the city during

327  a severe PM pollution episode occurred in December 2013. Wu et al. (2017) have also shown

328  that 61.5% of the $PM_{2.5}$ mass in Beijing is contributed by regional transport during a

329  summertime PM pollution episode. The contribution of Hebei emissions to the $PM_{2.5}$ mass in

330  Beijing is the most significant, exceeding 20% when Beijing's air quality is not excellent.

331  The contribution of emissions from Tianjin, Henan, Shandong, and Shanxi is generally less

332  than 10% under different pollution levels. However, when Beijing's air quality is severely

333  polluted, the contribution of Shandong emissions is also significant, attaining 16.4%. The

334  background source contributes more than 20% of the $PM_{2.5}$ mass in Beijing when the air

335  quality is excellent and severely polluted, and between 12.8% and 15.4% under the rest

336  pollution levels.

337  The air quality in Tianjin is dominated by trans-boundary transport of air pollutants,

338  with the non-local $PM_{2.5}$ contribution generally higher than 55%, especially when the air

Atmospheric
Chemistry
and Physics
Discussions

Open Access

EGU

339    quality is severely polluted, with the non-local $PM_{2.5}$ contribution of 95.9%, which is higher

340    than the average non-local contribution of 44% reported by Meng et al. (2020). The $PM_{2.5}$

341    contribution of local emissions decreases with the deterioration of the air quality in Tianjin,

342    with average contributions of 44.9%, 41.3%, 37.0%, and 29.6%, respectively, when the air

343    quality is good, slightly, moderately, and heavily polluted. The Hebei emissions play a

344    significant role in the PM pollution in Tianjin, generally contributing more than 25% of $PM_{2.5}$

345    concentrations, except when the air quality is excellent. Meng et al. (2020) have emphasized

346    the important contribution of Hebei emissions to $PM_{2.5}$ concentrations in Tianjin. However,

347    Meng et al. (2020) have suggested that the $PM_{2.5}$ contribution of local emissions gradually

348    increases with continuous deterioration of the PM pollution, which is different from that in

349    the study. The $PM_{2.5}$ contribution of the background source is between 11.4% to 16.5%,

350    except when the air quality is severely polluted, with the contribution exceeding 30%.

351      The Hebei's air quality is obviously determined by local emissions when the air quality

352    is excellent or good, with the average $PM_{2.5}$ contribution of 65.8% and 60.9%, respectively.

353    Additionally, the contribution of non-local emissions to the $PM_{2.5}$ mass in Hebei is almost the

354    same as that of local emissions, varying from 46.2% to 54.8% with $PM_{2.5}$ concentrations

355    exceeding 75 μg m$^{-3}$. The $PM_{2.5}$ contribution of emissions from Tianjin, Henan, and Shanxi is

356    generally less than 10% under different pollution levels. However, the Shandong emissions

357    contribute more than 10% of the $PM_{2.5}$ mass in Hebei when the air quality becomes polluted.

358    Obviously, with occurrence of severe PM pollution in BTH, the contribution of Shandong

359    emissions to the $PM_{2.5}$ mass in BTH becomes considerable, which has also been suggested by

360    Chang et al. (2019). The $PM_{2.5}$ contribution of background source to Hebei decreases with

361    deterioration of the air quality, ranging from 8.2% to 19.2% during the episode. Overall, in

362    Hebei, local emissions generally dominate the $PM_{2.5}$ level under different pollution level, but

363    non-local emissions play a more and more important role with deterioration of PM pollution,

Atmospheric
Chemistry
and Physics
Discussions

Open Access

EGU

**364** which is consistent with those in Wang et al. (2015) and Wang et al. (2019).

**365** The local and non-local emissions generally play an almost equivalent role in the air

**366** quality in Henan when the severe PM pollution does not occur. However, when the air quality

**367** is severely polluted, the non-local emissions contribute about 62% of the $PM_{2.5}$ mass. The

**368** Shandong emissions generally contribute more $PM_{2.5}$ mass than the other five provinces

**369** when the air quality is polluted, with the $PM_{2.5}$ contribution exceeding 10%. The background

**370** source accounts for more than 10% with the air quality being excellent or good. In Shandong,

**371** the local emissions dominate the air quality, generally contributing more than 60% of the

**372** $PM_{2.5}$ mass. The total $PM_{2.5}$ contribution of emissions from Beijing, Tianjin, Hebei, Henan,

**373** and Shanxi is less than 30%, and $PM_{2.5}$ contributions of background source range from 10%

**374** to 15% under different pollution levels. The air quality in Shanxi is mainly decided by local

**375** emissions, with the $PM_{2.5}$ contribution of 58.7%, 57.8%, 43.8%, and 47.7% when the air

**376** quality being from excellent, good, slightly, and moderately polluted, respectively. Hebei and

**377** Henan emissions contribute more than 10% and 15% of the $PM_{2.5}$ mass in Shanxi, when the

**378** air quality is slightly and moderately polluted. The $PM_{2.5}$ contribution of background source

**379** is notable, generally exceeding 20%.

**380** Table 4, Table 5 and Figure 10 further show the average contribution of local and

**381** non-local emissions to the aerosol species in Beijing, Tianjin, Hebei, Henan, Shandong, and

**382** Shanxi during the episode. Interestingly, the local emissions dominate the EC and POA in

**383** Beijing, with a contribution of 61.1% and 64.1%. Hu et al. (2015) have also revealed that

**384** local emissions constitute the major source of POA in Beijing, particularly during wintertime.

**385** Additionally, local emissions also account for around 32% of the SOA in Beijing, and the

**386** high organic aerosol contribution is likely caused by emissions of large amounts of vehicles

**387** in Beijing. Except for EC and POA, non-local emissions dominate the aerosol species

**388** concentration in Beijing, with contributions exceeding 60%, especially for sulfate and nitrate

389  in which the contribution of non-local emissions is more than 90% (Figure 10). Ying et al.

390  (2014) have shown that the inter-regional transport of air pollutants plays an important role in

391  the secondary aerosols formation during the polluted episode in China. Sun et al. (2016) have

392  also demonstrated that the secondary aerosol formed on a regional scale dominates the

393  aerosol compositions during the haze episode, with an average of 67%. Apparently, the

394  impact of Hebei emissions on PM pollution in Beijing is the most significant, with the nitrate

395  and ammonium contribution exceeding 40% (Table 4). Except for EC and POA,

396  contributions of background source to the aerosol species in Beijing is generally more than

397  10%. It is worth noting that the nitrate contribution of the background source is 32.1%, which

398  is caused by the slow oxidation of $NO_2$ during wintertime.

399       In Tianjin, the non-local emissions play a dominant role in concentrations SOA, sulfate,

400  nitrate, and ammonium, with contributions of 73.6%, 68.6%, 88.7%, and 71.3%, and also

401  account for 48.1% and 50.7% of the EC and POA mass, respectively. In general, Hebei

402  emissions constitute the most important contributor of aerosol species in the non-local

403  sources, followed by Shandong emissions. In Hebei, the local emissions determine the levels

404  of EC, POA, sulfate, and ammonium, with contributions of 73.8%, 63.0%, 64.3%, and 67.4%,

405  respectively. The SOA mass is mainly contributed by local (49.4%) and Shandong (16.7%)

406  emissions, and background sources (11.6%). However, the non-local emissions dominate the

407  nitrate mass in Hebei, with the contribution of 78.7%, most of which is from Henan (11.4%),

408  Shandong (14.6%), Shanxi (10.8%), and background sources (22.9%). Except for sulfate, the

409  aerosol species in Henan are generally controlled by local emissions, with contributions

410  varying from 45% to 65%. The sulfate contribution of non-local emissions is 83.2%, mainly

411  contributed by Hebei (16.7%), Shandong (14.9%), Shanxi (12.1%), and background (22%).

412  The local emissions contribute about 60~80% of the aerosol species mass in Shandong,

413  except nitrate aerosols, which are dominated by non-local emissions with a contribution of

414 75.1%. More than 60% of EC, POA, sulfate and ammonium in Shanxi are formed from local

415 emissions, but the non-local emissions are the dominant contributor to SOA and nitrate

416 concentrations.

417

418 **4    Summary and conclusions**

419 We have developed a source-oriented WRF-Chem model, treating the precursors of

420 aerosols from different sources and their corresponding reaction products as different species

421 and tracked independently in chemical, physical, and dynamic processes. The model is used

422 to evaluate contributions of local and non-local emissions to the PM pollution in the NCP,

423 including Beijing, Tianjin, Hebei, Henan, and Shandong, as well as the adjacent province on

424 the west, Shanxi during a persistent and severe haze episode from 05 December 2015 to 04

425 January 2016. The model exhibits good performance in predicting the temporal variation and

426 spatial distribution of air pollutants in the NCP and also reasonably simulates the aerosol

427 species against measurements in Beijing.

428 As two megacities in the NCP, Beijing and Tianjin have made great efforts to decrease

429 local emissions of air pollutants since 2013, such as replace residential coal use with gas and

430 electricity, elevating vehicle emissions standards, phasing out high-emitting industries, et al.

431 (Zhang et al., 2019). However, heavy PM pollutions still occur in the two cities, which is

432 mainly resulted from trans-boundary transport of air pollutants. Simulations of the

433 source-oriented WRF-Chem model reveal that, on average local and non-local emissions

434 contribute 36.3% and 63.7% of the $PM_{2.5}$ mass in Beijing during the episode. When the air

435 quality is excellent or good in terms of hourly $PM_{2.5}$ concentrations, the local emissions

436 contribute more than 50% to the $PM_{2.5}$ mass, dominating Beijing's air quality. However, with

437 deterioration of Beijing's air quality from being slightly to severely polluted, the $PM_{2.5}$

438 contribution of local emissions decreases from 48.7% to 25.1%, indicating the significant

Atmospheric
Chemistry
and Physics
Discussions

439    contribution of trans-boundary transport to the PM pollution in Beijing. The non-local

440    emissions account for 76.2% of the $PM_{2.5}$ mass in Tianjin and the contribution exceeds 90%

441    when the air quality is severely polluted. The $PM_{2.5}$ concentrations in three industrialized

442    provinces, Hebei, Shandong, and Henan in the NCP, are generally dominated by the local

443    emissions under different pollution levels, particularly in Shandong with the $PM_{2.5}$

444    contribution of local emissions exceeding 60%. Efficient emission mitigations of air

445    pollutants in the three provinces need to be carried out continuously to lower PM levels.

446    However, when severe PM pollution occurs, the $PM_{2.5}$ contribution of local emissions in

447    Hebei and Henan decreases considerably. The impact of Shanxi's emissions on $PM_{2.5}$

448    concentrations in the NCP is generally not significant.

449      The primary aerosol species, such as EC and POA, are generally controlled by local

450    emissions with the average contribution ranging from about 50% to 85% in the six provinces.

451    However, the source apportionment of secondary aerosols shows large differences during the

452    episode, with more evident regional characteristics. Local emissions contribute more than 60%

453    of the SOA mass in Shandong, 40~50% in Hebei, Henan and Shanxi, and around 30% in

454    Beijing and Tianjin. The sulfate contribution of local emissions is significant in Hebei,

455    Shandong and Shanxi, exceeding 60%, but less than 10% in Beijing. Except in Henan, local

456    emissions do not play an important role in the nitrate formation, with contributions less than

457    30%, and most of nitrate aerosols are produced during trans-boundary transport of its

458    precursors. Ammonium aerosols in Beijing and Tianjin are mainly determined by non-local

459    emissions, with the contribution of around 70%. Local emissions in the other four provinces

460    account for around 60% of the ammonium mass.

461      In order to reduce PM pollution, the cooperation to carry out strict emission mitigation

462    measures is critical for all provinces, especially with regard to Beijing and Tianjin. In Beijing

463    and Tianjin, reducing direct emissions of primary aerosols, such as EC and POA, constitutes

Atmospheric
Chemistry
and Physics
Discussions

464    the priority, and more efforts need to be made to reduce local emissions of air pollutants in

465    Hebei, Henan, Shandong, and Shanxi.

466

467    *Competing interests.* The authors declare no competing financial interest.

468

469    *Data availability.* The real-time $PM_{2.5}$, $O_3$, $NO_2$, $SO_2$ and CO observations are accessible for

470    the public on the following website: http://106.37.208. 233:20035/ (last access: 24 November

471    2019) (China MEP, 2013a). One can also access the historic profile of observed ambient

472    pollutants by visiting http://www.aqistudy.cn/ (last access: 24 November 2019) (China MEP,

473    2013b).

474

475    *Author contribution.* Guohui Li, as the contact author, provided the ideas and financial

476    support, developed the model code, verified the conclusions, and revised the paper. Jiarui Wu

477    conducted a research, designed the experiments, performed the simulation, processed the data,

478    prepared the data visualization, and prepared the manuscript with contributions from all

479    authors. Naifang Bei validated the model performance, analyzed the study data, and reviewed

480    the manuscript. Yuan Wang validated the model performance, verified the results and

481    provided the critical reviews. Suixin Liu provided the data and the primary data process, and

482    reviewed the manuscript. Xia Li, Lang Liu, Ruonan Wang, Jiaoyang Yu and Min Zuo

483    analyzed the initial simulation data, visualized the model results and reviewed the paper.

484    Zhenxing Shen, Junji Cao and Xuexi Tie provided critical reviews pre-publication stage.

485

# References

An, Z. S., Huang, R. J., Zhang, R. Y., Tie, X. X., Li, G. H., Cao, J. J., Zhou, W. J., Shi, Z. G., Han, Y. M., Gu, Z. L., and Ji, Y. M.: Severe haze in northern China: A synergy of anthropogenic emissions and atmospheric processes, P. Natl. Acad. Sci. USA., 116, 8657-8666, doi: 10.1073/pnas.1900125116, 2019.

Bei, N. F., Wu, J. R., Elser, M., Feng, T., Cao, J. J., El-Haddad, I., Li, X., Huang, R. J., Li, Z. Q., Long, X., Xing, L., Zhao, S. Y., Tie, X. X., Prevot, A. S. H., and Li, G. H.: Impacts of meteorological uncertainties on the haze formation in Beijing-Tianjin-Hebei (BTH) during wintertime: a case study, Atmos. Chem. Phys., 17, 14579-14591, 10.5194/acp-17-14579-2017, 2017.

Binkowski, F. S., and Roselle, S. J.: Models-3 community multiscale air quality (CMAQ) model aerosol component - 1. Model description, J. Geophys. Res. Atmos., 108, 18, doi: 10.1029/2001jd001409, 2003.

Burr, M. J., and Zhang, Y.: Source apportionment of fine particulate matter over the Eastern U.S. Part II: source apportionment simulations using CAMx/PSAT and comparisons with CMAQ source sensitivity simulations, Atmos. Pollut. Res., 2, 318-336, doi: 10.5094/apr.2011.037, 2011.

Carter, W. P. L.: Development of the SAPRC-07 chemical mechanism, Atmos. Environ., 44, 5324-5335, doi: 10.1016/j.atmosenv.2010.01.026, 2010.

Chang, X., Wang, S. X., Zhao, B., Xing, J., Liu, X. X., Wei, L., Song, Y., Wu, W. J., Cai, S. Y., Zheng, H. T., Ding, D., and Zheng, M.: Contributions of inter-city and regional transport to $PM_{2.5}$ concentrations in the Beijing-Tianjin-Hebei region and its implications on regional joint air pollution control, Sci. Total Environ., 660, 1191-1200, 10.1016/j.scitotenv.2018.12.474, 2019.

Chen, F., and Dudhia, J.: Coupling an advanced land surface-hydrology model with the Penn State-NCAR MM5 modeling system. Part I: Model implementation and sensitivity, Mon. Weather. Rev., 129, 569-585, doi: 10.1175/1520-0493(2001)129<0569:caalsh>2.0.co;2, 2001.

China MEP (Ministry of Environmental Protection, China): Air Quality Observation Real-time Release Platform of MEP Data Center, available at: http://106.37.208.233:20035/ (last access: 24 November 2019), 2013a.

China MEP (Ministry of Environmental Protection, China): On- line Monitoring and Analysis Platform of China Air Quality, available at: http://www.aqistudy.cn/ (last access: 24 November 2019), 2013b.

Chou, M.-D. and Suarez, M. J.: A solar radiation parameterization for atmospheric studies, NASA Tech. Rep. NASA/TM-1999- 10460, Vol. 15, 38 pp., 1999.

Chou, M.-D. and Suarez, M. J.: A thermal infrared radiation parameterization for atmospheric studies, NASA/TM-2001-104606, Vol. 19, 55 pp., 2001.

Cooper, J. A., and Watson, J. G.: Receptor oriented methods of air particulate source apportionment, J. Air. Pollut. Control. Assoc., 30, 1116-1125, doi: 10.1080/00022470.1980.10465157, 1980.

Donahue, N. M., Robinson, A. L., Stanier, C. O., and Pandis, S. N.: Coupled partitioning, dilution, and chemical aging of semivolatile organics, Environ. Sci. Technol., 40,

Atmospheric
Chemistry
and Physics
Discussions

Open Access

EGU

533 2635-2643, doi: 10.1021/es052297c, 2006.

534 Dong, Z., Wang, S., Xing, J., Chang, X., Ding, D., and Zheng, H.: Regional transport in
535  Beijing-Tianjin-Hebei region and its changes during 2014–2017: The impacts of
536  meteorology and emission reduction, Sci. Total Environ., 737, 139792,
537  https://doi.org/10.1016/j.scitotenv.2020.139792, 2020.

538 Feng, T., Bei, N. F., Huang, R. J., Cao, J. J., Zhang, Q., Zhou, W. J., Tie, X. X., Liu, S. X.,
539  Zhang, T., Su, X. L., Lei, W. F., Molina, L. T., and Li, G. H.: Summertime ozone
540  formation in Xi'an and surrounding areas, China, Atmos. Chem. Phys., 16, 4323-4342,
541  doi: 10.5194/acp-16-4323-2016, 2016.

542 Foley, K. M., Roselle, S. J., Appel, K. W., Bhave, P. V., Pleim, J. E., Otte, T. L., Mathur, R.,
543  Sarwar, G., Young, J. O., Gilliam, R. C., Nolte, C. G., Kelly, J. T., Gilliland, A. B., and
544  Bash, J. O.: Incremental testing of the Community Multiscale Air Quality (CMAQ)
545  modeling system version 4.7, Geosci. Model. Dev., 3, 205-226, doi:
546  10.5194/gmd-3-205-2010, 2010.

547 Grell, G. A., and Devenyi, D.: A generalized approach to parameterizing convection
548  combining ensemble and data assimilation techniques, Geophys. Res. Lett., 29, 4, doi:
549  10.1029/2002gl015311, 2002.

550 Grell, G. A., Peckham, S. E., Schmitz, R., McKeen, S. A., Frost, G., Skamarock, W. C., and
551  Eder, B.: Fully coupled "online" chemistry within the WRF model, Atmos. Environ., 39,
552  6957-6975, doi: 10.1016/j.atmosenv.2005.04.027, 2005.

553 Guenther, A., Karl, T., Harley, P., Wiedinmyer, C., Palmer, P. I., and Geron, C.: Estimates of
554  global terrestrial isoprene emissions using MEGAN (Model of Emissions of Gases and
555  Aerosols from Nature), Atmos. Chem. Phys., 6, 3181-3210, doi:
556  10.5194/acp-6-3181-2006, 2006a.

557 Guenther, A., Karl, T., Harley, P., Wiedinmyer, C., Palmer, P. I., and Geron, C.: Estimates of
558  global terrestrial isoprene emissions using MEGAN (Model of Emissions of Gases and
559  Aerosols from Nature), Atmos. Chem. Phys., 6, 3181-3210, 2006b.

560 Guo, S., Hu, M., Wang, Z. B., Slanina, J., and Zhao, Y. L.: Size-resolved aerosol
561  water-soluble ionic compositions in the summer of Beijing: implication of regional
562  secondary formation, Atmos. Chem. Phys., 10, 947-959, doi: 10.5194/acp-10-947-2010,
563  2010.

564 Guo, S., Hu, M., Zamora, M. L., Peng, J. F., Shang, D. J., Zheng, J., Du, Z. F., Wu, Z., Shao,
565  M., Zeng, L. M., Molina, M. J., and Zhang, R. Y.: Elucidating severe urban haze
566  formation in China, P. Natl. Acad. Sci. USA., 111, 17373-17378, doi:
567  10.1073/pnas.1419604111, 2014.

568 Hess, P. G., Flocke, S., Lamarque, J. F., Barth, M. C., and Madronich, S.: Episodic modeling
569  of the chemical structure of the troposphere as revealed during the spring MLOPEX 2
570  intensive, J. Geophys. Res. Atmos., 105, 26809-26839, doi: 10.1029/2000jd900253,
571  2000.

572 Hong, S.-Y., and Lim, J.-O. J.: The WRF Single-Moment 6-Class Microphysics Scheme
573  (WSM6), Asia-Pac. J. Atmos. Sci., 42, 129-151, 2006.

574 Horowitz, L. W., Walters, S., Mauzerall, D. L., Emmons, L. K., Rasch, P. J., Granier, C., Tie,
575  X. X., Lamarque, J. F., Schultz, M. G., Tyndall, G. S., Orlando, J. J., and Brasseur, G. P.:

576    A global simulation of tropospheric ozone and related tracers: Description and
577    evaluation of MOZART, version 2, J. Geophys. Res. Atmos., 108, 29, doi:
578    10.1029/2002jd002853, 2003.

579  Hu, J. L., Wu, L., Zheng, B., Zhang, Q., He, K. B., Chang, Q., Li, X. H., Yang, F. M., Ying,
580    Q., and Zhang, H. L.: Source contributions and regional transport of primary particulate
581    matter in China, Environ. Pollut., 207, 31-42, doi: 10.1016/j.envpol.2015.08.037, 2015.

582  Janjić, Z. I.: Nonsingular Implementation of the Mellor–Yamada Level 2.5 Scheme in the
583    NCEP Meso Model, Ncep Office Note, 436, 2002.

584  Jiang, C., Wang, H., Zhao, T., Li, T., and Che, H.: Modeling study of $PM_{2.5}$ pollutant
585    transport across cities in China's Jing-Jin- Ji region during a severe haze episode in
586    December 2013, Atmos. Chem. Phys., 15, 5803–5814, doi:10.5194/acp-15-5803-2015,
587    2015.

588  Lang, J. L., Cheng, S. Y., Li, J. B., Chen, D. S., Zhou, Y., Wei, X., Han, L. H., and Wang, H.
589    Y.: A Monitoring and Modeling Study to Investigate Regional Transport and
590    Characteristics of $PM_{2.5}$ Pollution, Aerosol. Air. Qual. Res., 13, 943-956, doi:
591    10.4209/aaqr.2012.09.0242, 2013.

592  Li, G., Lei, W., Zavala, M., Volkamer, R., Dusanter, S., Stevens, P., and Molina, L. T.:
593    Impacts of HONO sources on the photochemistry in Mexico City during the
594    MCMA-2006/MILAGO Campaign, Atmos. Chem. Phys., 10, 6551-6567, doi:
595    10.5194/acp-10-6551-2010, 2010.

596  Li, G., Bei, N., Tie, X., and Molina, L. T.: Aerosol effects on the photochemistry in Mexico
597    City during MCMA-2006/MILAGRO campaign, Atmos. Chem. Phys., 11, 5169-5182,
598    doi: 10.5194/acp-11-5169-2011, 2011a.

599  Li, G., Zavala, M., Lei, W., Tsimpidi, A. P., Karydis, V. A., Pandis, S. N., Canagaratna, M.
600    R., and Molina, L. T.: Simulations of organic aerosol concentrations in Mexico City
601    using the WRF-CHEM model during the MCMA-2006/MILAGRO campaign, Atmos.
602    Chem. Phys., 11, 3789-3809, doi: 10.5194/acp-11-3789-2011, 2011b.

603  Li, G. H., Zhang, R. Y., Fan, J. W., and Tie, X. X.: Impacts of black carbon aerosol on
604    photolysis and ozone, J. Geophys. Res. Atmos., 110, 10, doi: 10.1029/2005jd005898,
605    2005.

606  Li, G. H., Bei, N. F., Cao, J. J., Wu, J. R., Long, X., Feng, T., Dai, W. T., Liu, S. X., Zhang,
607    Q., and Tie, X. X.: Widespread and persistent ozone pollution in eastern China during
608    the non-winter season of 2015: observations and source attributions, Atmos. Chem.
609    Phys., 17, 2759-2774, doi: 10.5194/acp-17-2759-2017, 2017.

610  Li, P. F., Yan, R. C., Yu, S. C., Wang, S., Liu, W. P., and Bao, H. M.: Reinstate regional
611    transport of PM2.5 as a major cause of severe haze in Beijing, P. Natl. Acad. Sci. USA.,
612    112, E2739-E2740, doi: 10.1073/pnas.1502596112, 2015.

613  Li, X., Wu, J. R., Elser, M., Feng, T., Cao, J. J., El-Haddad, I., Huang, R. J., Tie, X. X.,
614    Prevot, A. S. H., and Li, G. H.: Contributions of residential coal combustion to the air
615    quality in Beijing-Tianjin-Hebei (BTH), China: a case study, Atmos. Chem. Phys., 18,
616    10675-10691, 10.5194/acp-18-10675-2018, 2018.

617  Lipsky, E. M., and Robinson, A. L.: Effects of dilution on fine particle mass and partitioning
618    of semivolatile organics in diesel exhaust and wood smoke, Environ. Sci. Technol., 40,

155-162, doi: 10.1021/es050319p, 2006.

Liu, L., Wang, L., Bai, Y., Yang, H., Lin, C., Kong, H., Ma, S., and Wang, J.: Simulation for the impacts of regional transport on winter particulate matter levels over Henan based on WRF/Chem model, Acta Scientiae Circumstantiae, 37, 1843-1854, 2017.

Long, X., Tie, X. X., Cao, J. J., Huang, R. J., Feng, T., Li, N., Zhao, S. Y., Tian, J., Li, G. H., and Zhang, Q.: Impact of crop field burning and mountains on heavy haze in the North China Plain: a case study, Atmos. Chem. Phys., 16, 9675-9691, doi: 10.5194/acp-16-9675-2016, 2016.

Marmur, A., Unal, A., Mulholland, J. A., and Russell, A. G.: Optimization-based source apportionment of PM$_{2.5}$ incorporating gas-to-particle ratios, Environ. Sci. Technol., 39, 3245-3254, doi: 10.1021/es0490121, 2005.

Marmur, A., Park, S. K., Mulholland, J. A., Tolbert, P. E., and Russell, A. G.: Source apportionment of PM$_{2.5}$ in the southeastern United States using receptor and emissions-based models: Conceptual differences and implications for time-series health studies, Atmos. Environ., 40, 2533-2551, doi: 10.1016/j.atmosenv.2005.12.019, 2006.

Meng, L., Cai, Z., Li, Y., Hao, J., and Wang, X.: Spatial and Temporal Distributions and Source Simulation during Heavy Pollution of PM$_{2.5}$ in Tianjin City, Research of Environmental Sciences, 33, 9-17, 2020.

Nenes, A., Pandis, S. N., and Pilinis, C.: ISORROPIA: A new thermodynamic equilibrium model for multiphase multicomponent inorganic aerosols, Aquat. Geochem., 4, 123-152, doi: 10.1023/a:1009604003981, 1998.

Odum, J. R., Hoffmann, T., Bowman, F., Collins, D., Flagan, R. C., and Seinfeld, J. H.: Gas/particle partitioning and secondary organic aerosol yields, Environ. Sci. Technol., 30, 2580-2585, doi: 10.1021/es950943+, 1996.

Paatero, P., and Tapper, U.: Analysis of different modes of factor-analysis as least-squares fit problems, Chemometrics Intell. Lab. Syst., 18, 183-194, doi: 10.1016/0169-7439(93)80055-m, 1993.

Pankow, J. F.: An absorption-model of the gas aerosol partitioning involved in the formation of secondary organic aerosol, Atmos. Environ., 28, 189-193, doi: 10.1016/1352-2310(94)90094-9, 1994.

Robinson, A. L., Donahue, N. M., Shrivastava, M. K., Weitkamp, E. A., Sage, A. M., Grieshop, A. P., Lane, T. E., Pierce, J. R., and Pandis, S. N.: Rethinking organic aerosols: Semivolatile emissions and photochemical aging, Science., 315, 1259-1262, doi: 10.1126/science.1133061, 2007.

Shrivastava, M. K., Lipsky, E. M., Stanier, C. O., and Robinson, A. L.: Modeling semivolatile organic aerosol mass emissions from combustion systems, Environ. Sci. Technol., 40, 2671-2677, doi: 10.1021/es0522231, 2006.

Shrivastava, M. K., Lane, T. E., Donahue, N. M., Pandis, S. N., and Robinson, A. L.: Effects of gas particle partitioning and aging of primary emissions on urban and regional organic aerosol concentrations, J. Geophys. Res. Atmos., 113, 16, doi: 10.1029/2007jd009735, 2008.

Sun, Y. L., Chen, C., Zhang, Y. J., Xu, W. Q., Zhou, L. B., Cheng, X. L., Zheng, H. T., Ji, D. S., Li, J., Tang, X., Fu, P. Q., and Wang, Z. F.: Rapid formation and evolution of an

662   extreme haze episode in Northern China during winter 2015, Sci. Rep., 6, 9, doi:
663       10.1038/srep27151, 2016.

664   Tsimpidi, A. P., Karydis, V. A., Zavala, M., Lei, W., Molina, L., Ulbrich, I. M., Jimenez, J.
665       L., and Pandis, S. N.: Evaluation of the volatility basis-set approach for the simulation of
666       organic aerosol formation in the Mexico City metropolitan area, Atmos. Chem. Phys.,
667       10, 525-546, doi: 10.5194/acp-10-525-2010, 2010.

668   Volkamer, R., Martini, F. S., Molina, L. T., Salcedo, D., Jimenez, J. L., and Molina, M. J.: A
669       missing sink for gas-phase glyoxal in Mexico City: Formation of secondary organic
670       aerosol, Geophys. Res. Lett., 34, 5, doi: 10.1029/2007gl030752, 2007.

671   Wagstrom, K. M., Pandis, S. N., Yarwood, G., Wilson, G. M., and Morris, R. E.:
672       Development and application of a computationally efficient particulate matter
673       apportionment algorithm in a three-dimensional chemical transport model, Atmos.
674       Environ., 42, 5650-5659, doi: 10.1016/j.atmosenv.2008.03.012, 2008.

675   Wang, L. T., Wei, Z., Wei, W., Fu, J. S., Meng, C. C., and Ma, S. M.: Source apportionment
676       of PM$_{2.5}$ in top polluted cities in Hebei, China using the CMAQ model, Atmos. Environ.,
677       122, 723-736, 10.1016/j.atmosenv.2015.10.041, 2015.

678   Wang, Q., Luo, K., Fan, J. R., Gao, X., and Cen, K. F.: Spatial Distribution and Multiscale
679       Transport Characteristics of PM$_{2.5}$ in China, Aerosol Air Qual. Res., 19, 1993-2007,
680       10.4209/aaqr.2019.04.0202, 2019.

681   Wang, Z. S., Chien, C. J., and Tonnesen, G. S.: Development of a tagged species source
682       apportionment algorithm to characterize three-dimensional transport and transformation
683       of precursors and secondary pollutants, J. Geophys. Res. Atmos., 114, 17, doi:
684       10.1029/2008jd010846, 2009.

685   Wesely, M. L.: Parameterization of surface resistances to gaseous dry deposition in
686       regional-scale numerical models , Atmos. Environ., 23, 1293-1304, 1989.

687   Wu, J. R., Li, G. H., Cao, J. J., Bei, N. F., Wang, Y. C., Feng, T., Huang, R. J., Liu, S. X.,
688       Zhang, Q., and Tie, X. X.: Contributions of trans-boundary transport to summertime air
689       quality in Beijing, China, Atmos. Chem. Phys., 17, 2035-2051, doi:
690       10.5194/acp-17-2035-2017, 2017.

691   Wu, J. R., Bei, N. F., Hu, B., Liu, S. X., Wang, Y., Shen, Z. X., Li, X., Liu, L., Wang, R. N.,
692       Liu, Z. R., Cao, J. J., Tie, X. X., Molina, L. T., and Li, G. H.: Aerosol-photolysis
693       interaction reduces particulate matter during wintertime haze events, P. Natl. Acad. Sci.
694       USA., 117, 9755-9761, 10.1073/pnas.1916775117, 2020.

695   Ying, Q., and Kleeman, M. J.: Source contributions to the regional distribution of secondary
696       particulate matter in California, Atmos. Environ., 40, 736-752, doi:
697       10.1016/j.atmosenv.2005.10.007, 2006.

698   Ying, Q., Lu, J., Allen, P., Livingstone, P., Kaduwela, A., and Kleeman, M.: Modeling air
699       quality during the California Regional PM$_{10}$/PM$_{2.5}$ Air Quality Study (CRPAQS) using
700       the UCD/CIT source-oriented air quality model - Part I. Base case model results, Atmos.
701       Environ., 42, 8954-8966, doi: 10.1016/j.atmosenv.2008.05.064, 2008a.

702   Ying, Q., Lu, J., Kaduwela, A., and Kleeman, M.: Modeling air quality during the California
703       Regional PM$_{10}$/PM$_{2.5}$ Air Quality Study (CPRAQS) using the UCD/CIT Source Oriented
704       Air Quality Model - Part II. Regional source apportionment of primary airborne

Atmospheric
Chemistry
and Physics
Discussions

705     particulate matter, Atmos. Environ., 42, 8967-8978, doi:
706     10.1016/j.atmosenv.2008.05.065, 2008b.

707 Ying, Q., Wu, L., and Zhang, H. L.: Local and inter-regional contributions to $PM_{2.5}$ nitrate
708     and sulfate in China, Atmos. Environ., 94, 582-592, doi:
709     10.1016/j.atmosenv.2014.05.078, 2014.

710 Zamora, M. L., Peng, J., Hu, M., Guo, S., Marrero-Ortiz, W., Shang, D., Zheng, J., Du, Z.,
711     Wu, Z., and Zhang, R.: Wintertime aerosol properties in Beijing, Atmos. Chem. Phys.,
712     19, 14329-14338, doi: 10.5194/acp-19-14329-2019, 2019.

713 Zhang, H., DeNero, S. P., Joe, D. K., Lee, H. H., Chen, S. H., Michalakes, J., and Kleeman,
714     M. J.: Development of a source oriented version of the WRF/Chem model and its
715     application to the California regional $PM_{10}/PM_{2.5}$ air quality study, Atmos. Chem. Phys.,
716     14, 485-503, doi: 10.5194/acp-14-485-2014, 2014.

717 Zhang, H. L., and Ying, Q.: Source apportionment of airborne particulate matter in Southeast
718     Texas using a source-oriented 3D air quality model, Atmos. Environ., 44, 3547-3557,
719     doi: 10.1016/j.atmosenv.2010.06.004, 2010.

720 Zhang, H. L., and Ying, Q.: Secondary organic aerosol formation and source apportionment
721     in Southeast Texas, Atmos. Environ., 45, 3217-3227, doi:
722     10.1016/j.atmosenv.2011.03.046, 2011.

723 Zhang, Q., Streets, D. G., Carmichael, G. R., He, K. B., Huo, H., Kannari, A., Klimont, Z.,
724     Park, I. S., Reddy, S., Fu, J. S., Chen, D., Duan, L., Lei, Y., Wang, L. T., and Yao, Z. L.:
725     Asian emissions in 2006 for the NASA INTEX-B mission, Atmos. Chem. Phys., 9,
726     5131-5153, 2009.

727 Zhang, Q., Zheng, Y. X., Tong, D., Shao, M., Wang, S. X., Zhang, Y. H., Xu, X. D., Wang, J.
728     N., He, H., Liu, W. Q., Ding, Y. H., Lei, Y., Li, J. H., Wang, Z. F., Zhang, X. Y., Wang,
729     Y. S., Cheng, J., Liu, Y., Shi, Q. R., Yan, L., Geng, G. N., Hong, C. P., Li, M., Liu, F.,
730     Zheng, B., Cao, J. J., Ding, A. J., Gao, J., Fu, Q. Y., Huo, J. T., Liu, B. X., Liu, Z. R.,
731     Yang, F. M., He, K. B., and Hao, J. M.: Drivers of improved $PM_{2.5}$ air quality in China
732     from 2013 to 2017, P. Natl. Acad. Sci. USA., 116, 24463-24469,
733     10.1073/pnas.1907956116, 2019.

734 Zhang, R. Y., Guo, S., Zamora, M. L., and Hu, M.: Reply to Li et al.: Insufficient evidence
735     for the contribution of regional transport to severe haze formation in Beijing, P. Natl.
736     Acad. Sci. USA., 112, E2741-E2741, doi: 10.1073/pnas.1503855112, 2015.

737 Zheng, B., Tong, D., Li, M., Liu, F., Hong, C. P., Geng, G. N., Li, H. Y., Li, X., Peng, L. Q.,
738     Qi, J., Yan, L., Zhang, Y. X., Zhao, H. Y., Zheng, Y. X., He, K. B., and Zhang, Q.:
739     Trends in China's anthropogenic emissions since 2010 as the consequence of clean air
740     actions, Atmos. Chem. Phys., 18, 14095-14111, 10.5194/acp-18-14095-2018, 2018.

741 Zhao, J., Levitt, N. P., Zhang, R. Y., and Chen, J. M.: Heterogeneous reactions of
742     methylglyoxal in acidic media: Implications for secondary organic aerosol formation,
743     Environ. Sci. Technol. 40, 7682-7687, doi: 10.1021/es060610k, 2006.

744
745

746    Table 1 WRF-Chem model configurations.

747

| Region | North China Plain |
|---|---|
| Simulation period | 05 December 2015 to 04 January 2016 |
| Domain size | 300 × 300 |
| Domain center | 38°N, 116°E |
| Horizontal resolution | 6 km × 6 km |
| Vertical resolution | 35 vertical levels with a stretched vertical grid with spacing ranging from 30 m near the surface, to 500 m at 2.5 km and 1 km above 14 km |
| Microphysics scheme | WSM 6-class graupel scheme (Hong and Lim, 2006) |
| Cumulus scheme | Grell-Devenyi ensemble scheme (Grell and Devenyi, 2002) |
| Boundary layer scheme | MYJ TKE scheme(Janjić, 2002) |
| Surface layer scheme | MYJ surface scheme (Janjić, 2002) |
| Land-surface scheme | Unified Noah land-surface model (Chen and Dudhia, 2001) |
| Longwave radiation scheme | Goddard longwave scheme (Chou and Suarez, 2001) |
| Shortwave radiation scheme | Goddard shortwave scheme (Chou and Suarez, 1999) |
| Meteorological boundary and initial conditions | NCEP 1°×1° reanalysis data |
| Chemical initial and boundary conditions | MOZART 6-hour output (Horowitz et al., 2003) |
| Anthropogenic emission inventory | Developed by Zhang et al. (2009) and Li et al. (2017), 2012 base year, and SAPRC-99 chemical mechanism |
| Biogenic emission inventory | Online MEGAN model developed by Guenther et al. (2006) |

748
749
750
751
752

Atmospheric
Chemistry
and Physics
Discussions

Table 2 Average PM$_{2.5}$ contributions (%) in Beijing, Tianjin, and Hebei under different
pollution levels from local, the other five provinces, and background source from 05
December 2015 to 04 January 2016.

| Pollution Level ($\mu g\ m^{-3}$) | 0-35 | 35-75 | 75-115 | 115-150 | 150-250 | >250 |
|---|---|---|---|---|---|---|
| **Beijing** | | | | | | |
| Beijing | 56.8 | 55.0 | 48.7 | 40.5 | 35.4 | 25.1 |
| Tianjin | 1.1 | 3.7 | 5.2 | 9.3 | 8.0 | 8.0 |
| Hebei | 16.9 | 20.4 | 24.8 | 28.4 | 28.4 | 21.2 |
| Henan | 1.1 | 1.2 | 1.8 | 1.4 | 3.4 | 6.2 |
| Shandong | 1.1 | 1.2 | 2.0 | 2.4 | 7.1 | 16.4 |
| Shanxi | 2.2 | 3.0 | 3.8 | 2.9 | 4.8 | 2.5 |
| Background | 20.8 | 15.4 | 13.8 | 15.1 | 12.8 | 20.6 |
| **Tianjin** | | | | | | |
| Beijing | 21.6 | 7.8 | 5.7 | 5.9 | 7.8 | 8.8 |
| Tianjin | 36.5 | 44.9 | 41.3 | 37.0 | 29.6 | 4.1 |
| Hebei | 23.1 | 28.3 | 30.4 | 31.7 | 30.6 | 27.8 |
| Henan | 0.8 | 1.1 | 1.3 | 2.1 | 3.7 | 6.7 |
| Shandong | 0.8 | 2.0 | 3.6 | 6.2 | 13.9 | 18.0 |
| Shanxi | 0.8 | 1.3 | 1.6 | 2.3 | 3.0 | 4.1 |
| Background | 16.5 | 14.6 | 16.0 | 14.9 | 11.4 | 30.5 |
| **Hebei** | | | | | | |
| Beijing | 4.1 | 5.7 | 5.7 | 6.2 | 5.0 | 5.8 |
| Tianjin | 2.7 | 5.2 | 5.3 | 5.5 | 5.4 | 6.7 |
| Hebei | 65.8 | 60.9 | 53.8 | 50.3 | 45.2 | 49.0 |
| Henan | 0.9 | 3.1 | 5.4 | 5.8 | 9.3 | 6.7 |
| Shandong | 0.9 | 5.4 | 11.3 | 12.7 | 18.0 | 18.6 |
| Shanxi | 6.4 | 4.4 | 5.4 | 5.6 | 5.7 | 5.1 |
| Background | 19.2 | 15.2 | 13.1 | 13.9 | 11.3 | 8.2 |

**762**  Table 3 Same as Table 2, but for Henan, Shandong, and Shanxi.
**763**

| Pollution Level ($\mu g\ m^{-3}$) | 0-35 | 35-75 | 75-115 | 115-150 | 150-250 | >250 |
|---|---|---|---|---|---|---|
| **Henan** | | | | | | |
| Beijing | 0.1 | 1.2 | 1.5 | 2.2 | 2.4 | 2.7 |
| Tianjin | 0.2 | 1.2 | 1.5 | 2.3 | 2.3 | 3.1 |
| Hebei | 2.4 | 4.1 | 6.9 | 9.2 | 12.1 | 18.3 |
| Henan | 55.2 | 55.3 | 55.3 | 50.1 | 45.5 | 38.0 |
| Shandong | 2.8 | 6.5 | 11.3 | 13.5 | 13.1 | 20.0 |
| Shanxi | 12.9 | 8.2 | 4.7 | 5.0 | 5.0 | 5.9 |
| Background | 26.3 | 23.5 | 18.8 | 17.7 | 19.7 | 11.9 |
| **Shandong** | | | | | | |
| Beijing | 4.2 | 1.8 | 2.7 | 2.4 | 3.0 | 2.2 |
| Tianjin | 3.8 | 2.0 | 3.2 | 2.4 | 3.3 | 2.2 |
| Hebei | 11.8 | 11.5 | 9.6 | 5.5 | 9.6 | 5.2 |
| Henan | 3.5 | 3.5 | 4.4 | 6.1 | 8.6 | 10.1 |
| Shandong | 59.2 | 64.2 | 62.3 | 69.7 | 61.7 | 66.5 |
| Shanxi | 3.8 | 2.6 | 2.8 | 2.5 | 3.6 | 3.4 |
| Background | 13.8 | 14.4 | 15.2 | 11.3 | 10.3 | 10.3 |
| **Shanxi** | | | | | | |
| Beijing | 1.3 | 1.6 | 1.6 | 1.2 | / | / |
| Tianjin | 1.3 | 1.2 | 1.4 | 1.0 | / | / |
| Hebei | 1.8 | 7.2 | 10.3 | 10.0 | / | / |
| Henan | 1.8 | 7.9 | 18.0 | 17.7 | / | / |
| Shandong | 1.3 | 1.9 | 3.4 | 2.7 | / | / |
| Shanxi | 58.7 | 57.8 | 43.8 | 47.7 | / | / |
| Background | 33.6 | 22.3 | 21.5 | 19.7 | / | / |

**764**
**765**
**766**
**767**
**768**

Atmospheric
Chemistry
and Physics
Discussions

**769** Table 4 Average aerosol constituent contributions (%) in Beijing, Tianjin, and Hebei from
**770** local, the other five, and background source from 05 December 2015 to 04 January 2016.
**771**

| Species | EC | POA | SOA | Sulfate | Nitrate | Ammonium |
|---|---|---|---|---|---|---|
| **Beijing** | | | | | | |
| Beijing | 61.1 | 64.1 | 31.9 | 9.8 | 10.0 | 32.5 |
| Tianjin | 5.1 | 7.0 | 8.5 | 7.8 | 8.6 | 7.5 |
| Hebei | 24.9 | 19.0 | 29.1 | 48.0 | 19.1 | 40.8 |
| Henan | 0.6 | 0.7 | 2.1 | 3.9 | 8.6 | 2.5 |
| Shandong | 2.3 | 3.2 | 7.1 | 9.8 | 10.5 | 5.0 |
| Shanxi | 1.3 | 2.1 | 3.5 | 7.8 | 11.0 | 1.7 |
| Background | 4.6 | 3.9 | 17.7 | 12.7 | 32.1 | 10.0 |
| **Tianjin** | | | | | | |
| Beijing | 5.3 | 7.1 | 13.8 | 1.1 | 10.2 | 3.4 |
| Tianjin | 51.9 | 49.3 | 26.4 | 31.4 | 11.3 | 28.7 |
| Hebei | 23.7 | 18.7 | 23.8 | 27.7 | 19.4 | 31.5 |
| Henan | 2.3 | 2.8 | 5.2 | 6.5 | 11.1 | 6.8 |
| Shandong | 9.8 | 15.3 | 20.7 | 20.3 | 16.7 | 17.5 |
| Shanxi | 1.3 | 1.5 | 2.6 | 4.4 | 10.6 | 0.8 |
| Background | 5.9 | 5.3 | 7.5 | 8.6 | 20.6 | 11.2 |
| **Hebei** | | | | | | |
| Beijing | 4.4 | 7.2 | 6.0 | 0.8 | 9.4 | 2.4 |
| Tianjin | 3.7 | 4.8 | 5.3 | 3.1 | 9.5 | 3.2 |
| Hebei | 73.8 | 63.0 | 49.4 | 64.3 | 21.3 | 67.4 |
| Henan | 4.1 | 5.9 | 7.8 | 9.2 | 11.4 | 9.3 |
| Shandong | 6.5 | 11.4 | 16.7 | 12.6 | 14.6 | 9.7 |
| Shanxi | 2.4 | 3.0 | 3.2 | 5.0 | 10.8 | 1.2 |
| Background | 5.0 | 4.8 | 11.6 | 4.9 | 22.9 | 6.9 |

**772**
**773**
**774**
**775**
**776**

Atmospheric
Chemistry
and Physics
Discussions

777    Table 5 Same as Table 4, but for Henan, Shandong, and Shanxi.

778

| Species | EC | POA | SOA | Sulfate | Nitrate | Ammonium |
|---|---|---|---|---|---|---|
| **Henan** | | | | | | |
| Beijing | 0.6 | 0.5 | 1.1 | 8.7 | 0.2 | 0.6 |
| Tianjin | 0.7 | 0.6 | 0.8 | 8.7 | 0.4 | 0.7 |
| Hebei | 16.5 | 11.9 | 13.9 | 16.7 | 14.4 | 16.5 |
| Henan | 56.5 | 59.2 | 45.0 | 16.8 | 64.3 | 56.5 |
| Shandong | 8.6 | 12.1 | 14.4 | 14.9 | 7.9 | 8.6 |
| Shanxi | 5.4 | 6.1 | 4.9 | 12.1 | 2.0 | 5.4 |
| Background | 11.7 | 9.5 | 19.8 | 22.0 | 10.8 | 11.7 |
| **Shandong** | | | | | | |
| Beijing | 1.0 | 1.0 | 2.1 | 0.2 | 10.1 | 0.5 |
| Tianjin | 1.1 | 1.0 | 1.4 | 1.0 | 10.5 | 0.8 |
| Hebei | 7.5 | 4.5 | 6.5 | 7.1 | 16.5 | 7.3 |
| Henan | 5.1 | 5.1 | 7.9 | 8.7 | 13.8 | 10.2 |
| Shandong | 71.9 | 78.2 | 60.4 | 68.3 | 24.9 | 62.5 |
| Shanxi | 1.5 | 1.3 | 2.0 | 3.4 | 11.7 | 0.7 |
| Background | 11.8 | 8.9 | 19.6 | 11.3 | 12.6 | 18.0 |
| **Shanxi** | | | | | | |
| Beijing | 0.4 | 0.4 | 1.5 | 0.1 | 7.1 | 0.3 |
| Tianjin | 0.2 | 0.2 | 4.0 | 0.2 | 6.6 | 0.3 |
| Hebei | 5.3 | 3.2 | 8.6 | 5.5 | 13.7 | 9.3 |
| Henan | 4.9 | 4.4 | 14.1 | 10.4 | 15.3 | 16.3 |
| Shandong | 0.7 | 0.8 | 2.5 | 1.3 | 8.5 | 1.8 |
| Shanxi | 79.8 | 84.1 | 42.1 | 74.7 | 19.4 | 62.2 |
| Background | 8.8 | 6.8 | 27.1 | 7.8 | 29.5 | 9.7 |

779
780
781
782
783

**Figure Captions**

784

785

786 Figure 1 WRF-Chem simulation domain with topography. The blue circles represent centers
787 of cities with ambient monitoring sites, and the size of circles denotes the number of
788 ambient monitoring sites of cities. The red circle denotes observation site for aerosol
789 species at the National Center for Nanoscience and Technology (NCNST), Chinese
790 Academy of Sciences, Beijing.

791 Figure 2 Conceptual scheme of source apportionment for sulfate aerosols formed from (a)
792 homogenous and (b) heterogeneous reactions. *FR*: formation rate; Superscript *i*:
793 source number; Superscript *T*: total; Subscript *g*: gas phase; Subscript *a*: aerosol
794 phase.

795 Figure 3 Conceptual scheme of source apportionment for nitrate and ammonium aerosols.
796 Superscript *i*: source number; Superscript *T*: total; Subscript *g*: gas phase; Subscript *a*:
797 aerosol phase.

798 Figure 4 Conceptual scheme of source apportionment for organic aerosols formed from (a)
799 homogenous and (b) heterogeneous reactions. Superscript *i*: source number;
800 Superscript *T*: total; Subscripts *j* and *k*: volatility bin number; Subscript *g*: gas phase;
801 Subscript *a*: aerosol phase. AVOC/BVOC: VOCs emitted from
802 anthropogenic/biogenic source; ASVOC/BSVOC: SVOC from oxidation of
803 AVOC/BVOC; OPOG: oxidized POG. PSOA: SOA from oxidation and partitioning
804 of POA treated as semi-volatile; ASOA/BSOA: SOA from oxidation of
805 anthropogenic/biogenic VOCs; HSOA: SOA from irreversible uptake of glyoxal and
806 methylglyoxal on aerosol/cloud surfaces.

807 Figure 5 Comparison of observed (black dots) and simulated (solid red lines) diurnal profiles
808 of near-surface hourly mass concentrations of (a) $PM_{2.5}$, (b) $O_3$, (c) $NO_2$, (d) $SO_2$, and
809 (d) CO averaged at monitoring sites in the NCP from 05 December 2015 to 04
810 January 2016.

811 Figure 6 Pattern comparisons of simulated (color counters) vs. observed (colored circles)
812 near-surface mass concentrations of (a) $PM_{2.5}$, (b) $O_3$, (c) $NO_2$, and (d) $SO_2$ averaged
813 from 05 December 2015 to 04 January 2016. The black arrows indicate simulated
814 near-surface winds.

815 Figure 7 Comparison of measured (black dots) and simulated (black line) diurnal profiles of
816 submicron aerosol species of (a) POA, (b) SOA, (c) sulfate, (d) nitrate, and (e)
817 ammonium at NCNST site in Beijing from 05 December 2015 to 04 January 2016.

818 Figure 8 Spatial distribution of average $PM_{2.5}$ contributions from (a) Beijing, (b) Tianjin, (c)
819 Hebei, (d) Shandong, (e) Henan, and (f) Shanxi provinces from 05 December 2015 to
820 04 January 2016.

821 Figure 9 Average $PM_{2.5}$ contributions (%) in (a) Beijing, (b) Tianjin, (c) Hebei, (d) Henan, (e)
822 Shandong, and (f) Shanxi from local (red) and non-local (blue) emissions from 05
823 December 2015 to 04 January 2016 under different pollution levels.

824 Figure 10 Average aerosol constituent contributions (%) in (a) Beijing, (b) Tianjin, (c) Hebei,
825 (d) Henan, (e) Shandong, and (f) Shanxi from local (red) and non-local (blue)
826 emissions from 05 December 2015 to 04 January 2016.

827
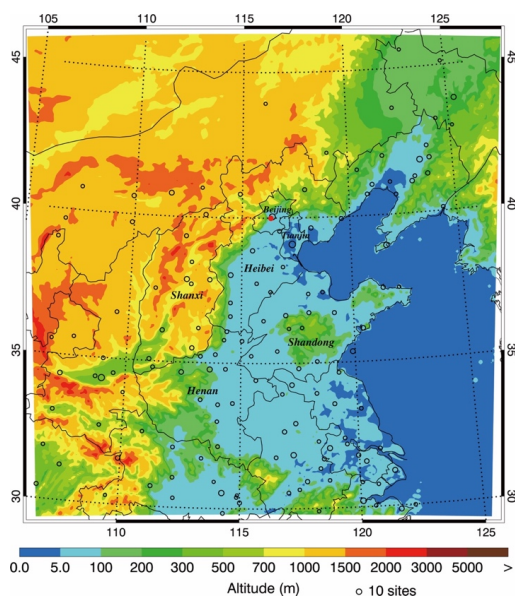
828

829

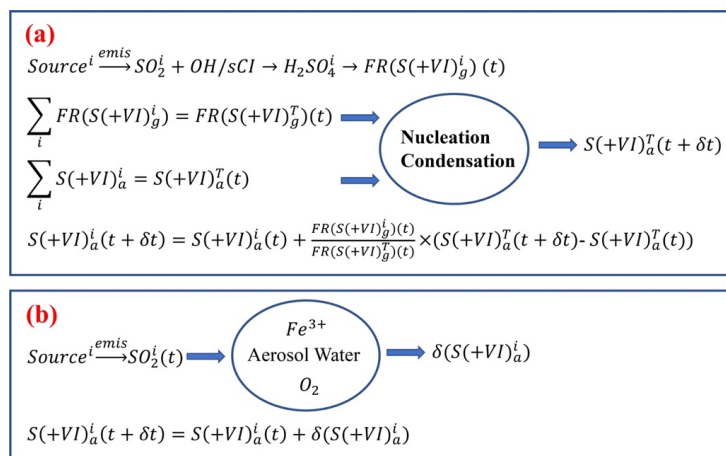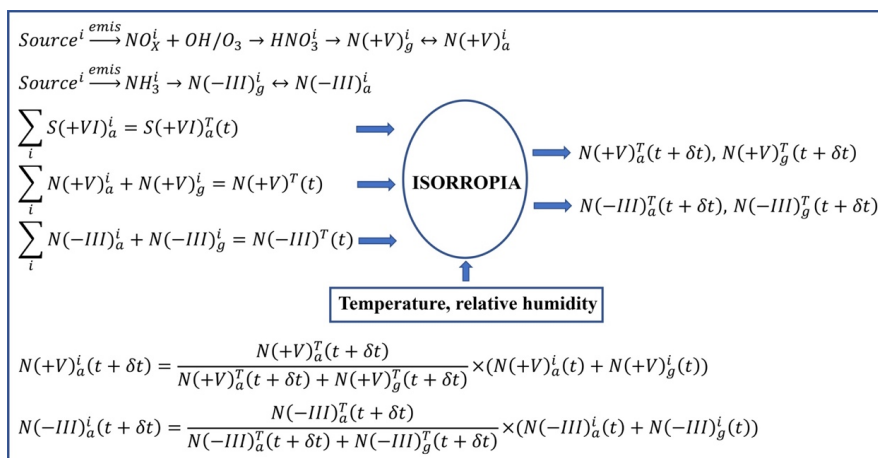830 Figure 1 WRF-Chem simulation domain with topography. The circles represent centers of
831 cities with ambient monitoring sites, and the size of blue circles denotes the number of
832 ambient monitoring sites of cities. The red circle denotes observation site for aerosol species
833 at the National Center for Nanoscience and Technology (NCNST), Chinese Academy of
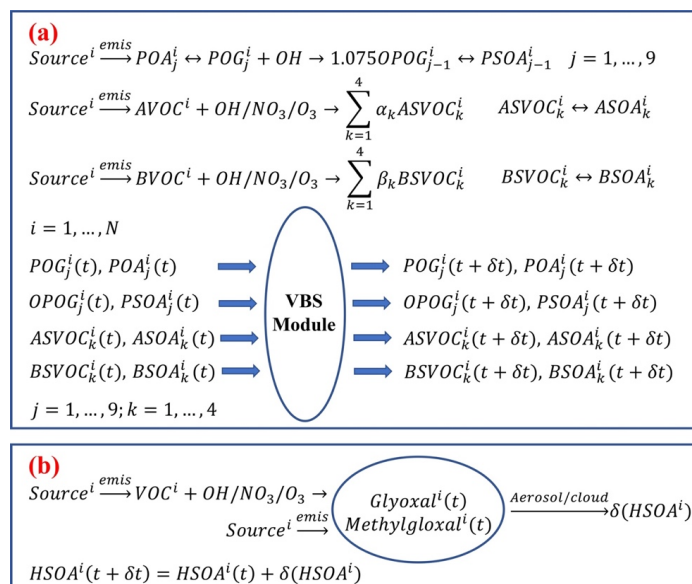834 Sciences, Beijing.

835

836

837

838

839

**(a)**

$$Source^i \xrightarrow{emis} SO_2^i + OH/sCI \rightarrow H_2SO_4^i \rightarrow FR(S(+VI)_g^i)(t)$$

$$\sum_i FR(S(+VI)_g^i) = FR(S(+VI)_g^T)(t)$$

Nucleation
Condensation

$$\sum_i S(+VI)_a^i = S(+VI)_a^T(t)$$

$$S(+VI)_a^T(t+\delta t)$$

$$S(+VI)_a^i(t+\delta t) = S(+VI)_a^i(t) + \frac{FR(S(+VI)_g^i)(t)}{FR(S(+VI)_g^T)(t)} \times (S(+VI)_a^T(t+\delta t) - S(+VI)_a^T(t))$$

**(b)**

$$Source^i \xrightarrow{emis} SO_2^i(t)$$

$Fe^{3+}$
Aerosol Water
$O_2$

$$\delta(S(+VI)_a^i)$$

$$S(+VI)_a^i(t+\delta t) = S(+VI)_a^i(t) + \delta(S(+VI)_a^i)$$

840
841
842 Figure 2 Conceptual scheme of source apportionment for sulfate aerosols formed from (a)
843 homogenous and (b) heterogeneous reactions. *FR*: formation rate; Superscript *i*: source
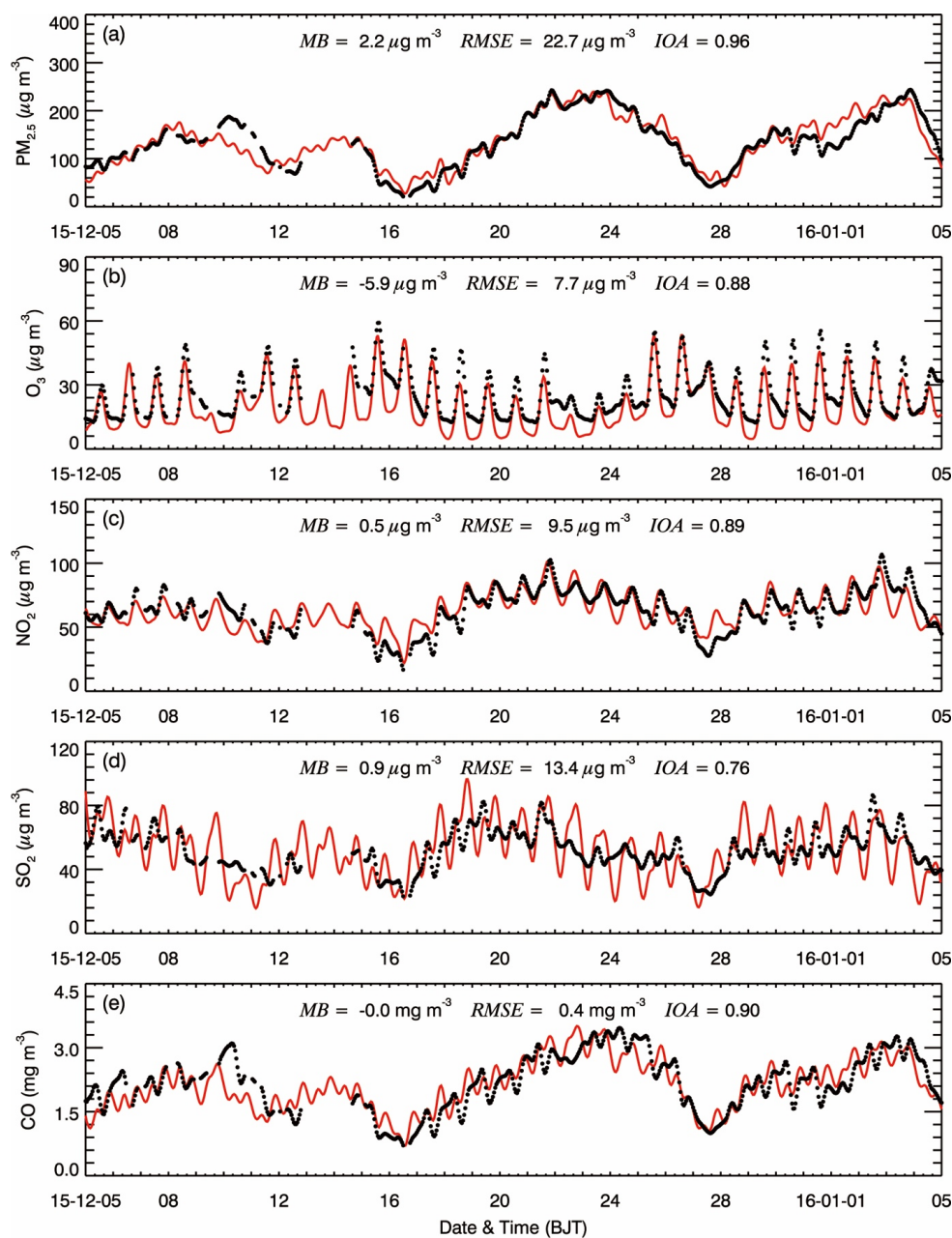844 number; Superscript *T*: total; Subscript *g*: gas phase; Subscript *a*: aerosol phase.
845
846
847
848
849

$$Source^i \xrightarrow{emis} NO_X^i + OH/O_3 \rightarrow HNO_3^i \rightarrow N(+V)_g^i \leftrightarrow N(+V)_a^i$$

$$Source^i \xrightarrow{emis} NH_3^i \rightarrow N(-III)_g^i \leftrightarrow N(-III)_a^i$$

$$\sum_i S(+VI)_a^i = S(+VI)_a^T(t)$$

$$\sum_i N(+V)_a^i + N(+V)_g^i = N(+V)^T(t) \longrightarrow \text{ISORROPIA}$$

$$\sum_i N(-III)_a^i + N(-III)_g^i = N(-III)^T(t)$$

$\longrightarrow N(+V)_a^T(t + \delta t), N(+V)_g^T(t + \delta t)$

$\longrightarrow N(-III)_a^T(t + \delta t), N(-III)_g^T(t + \delta t)$

**Temperature, relative humidity**

$$N(+V)_a^i(t + \delta t) = \frac{N(+V)_a^T(t + \delta t)}{N(+V)_a^T(t + \delta t) + N(+V)_g^T(t + \delta t)} \times (N(+V)_a^i(t) + N(+V)_g^i(t))$$

$$N(-III)_a^i(t + \delta t) = \frac{N(-III)_a^T(t + \delta t)}{N(-III)_a^T(t + \delta t) + N(-III)_g^T(t + \delta t)} \times (N(-III)_a^i(t) + N(-III)_g^i(t))$$

Figure 3 Conceptual scheme of source apportionment for nitrate and ammonium aerosols. Superscript *i*: source number; Superscript *T*: total; Subscript *g*: gas phase; Subscript *a*: aerosol phase.

Atmospheric
Chemistry
and Physics
Discussions
Open Access
EGU

**(a)**

$$Source^i \xrightarrow{emis} POA^i_j \leftrightarrow POG^i_j + OH \rightarrow 1.075 OPOG^i_{j-1} \leftrightarrow PSOA^i_{j-1} \quad j = 1, \dots, 9$$

$$Source^i \xrightarrow{emis} AVOC^i + OH/NO_3/O_3 \rightarrow \sum_{k=1}^{4} \alpha_k ASVOC^i_k \qquad ASVOC^i_k \leftrightarrow ASOA^i_k$$

$$Source^i \xrightarrow{emis} BVOC^i + OH/NO_3/O_3 \rightarrow \sum_{k=1}^{4} \beta_k BSVOC^i_k \qquad BSVOC^i_k \leftrightarrow BSOA^i_k$$

$$i = 1, \dots, N$$

$$POG^i_j(t), POA^i_j(t) \Rightarrow \qquad \Rightarrow POG^i_j(t+\delta t), POA^i_j(t+\delta t)$$

$$OPOG^i_j(t), PSOA^i_j(t) \Rightarrow \quad \boxed{\text{VBS Module}} \quad \Rightarrow OPOG^i_j(t+\delta t), PSOA^i_j(t+\delta t)$$

$$ASVOC^i_k(t), ASOA^i_k(t) \Rightarrow \qquad \Rightarrow ASVOC^i_k(t+\delta t), ASOA^i_k(t+\delta t)$$

$$BSVOC^i_k(t), BSOA^i_k(t) \Rightarrow \qquad \Rightarrow BSVOC^i_k(t+\delta t), BSOA^i_k(t+\delta t)$$

$$j = 1, \dots, 9; k = 1, \dots, 4$$

**(b)**

$$Source^i \xrightarrow{emis} VOC^i + OH/NO_3/O_3 \rightarrow \left( \begin{array}{c} Glyoxal^i(t) \\ Methylgloxal^i(t) \end{array} \right. \xrightarrow{Aerosol/cloud} \delta(HSOA^i)$$

$$Source^i \xrightarrow{emis}$$

$$HSOA^i(t+\delta t) = HSOA^i(t) + \delta(HSOA^i)$$

860
861
862 Figure 4 Conceptual scheme of source apportionment for organic aerosols formed from (a)
863 homogenous and (b) heterogeneous reactions. Superscript $i$: source number; Superscript $T$:
864 total; Subscripts $j$ and $k$: volatility bin number; Subscript $g$: gas phase; Subscript $a$: aerosol
865 phase. AVOC/BVOC: VOCs emitted from anthropogenic/biogenic source; ASVOC/BSVOC:
866 SVOC from oxidation of AVOC/BVOC; OPOG: oxidized POG. PSOA: SOA from oxidation
867 and partitioning of POA treated as semi-volatile; ASOA/BSOA: SOA from oxidation of
868 anthropogenic/biogenic VOCs; HSOA: SOA from irreversible uptake of glyoxal and
869 methylglyoxal on aerosol/cloud surfaces.
870
871
872
873
874

Figure 5 Comparison of observed (black dots) and simulated (solid red lines) diurnal profiles of near-surface hourly mass concentrations of (a) $PM_{2.5}$, (b) $O_3$, (c) $NO_2$, (d) $SO_2$, and (d) CO averaged at monitoring sites in the NCP from 05 December 2015 to 04 January 2016.

Atmospheric
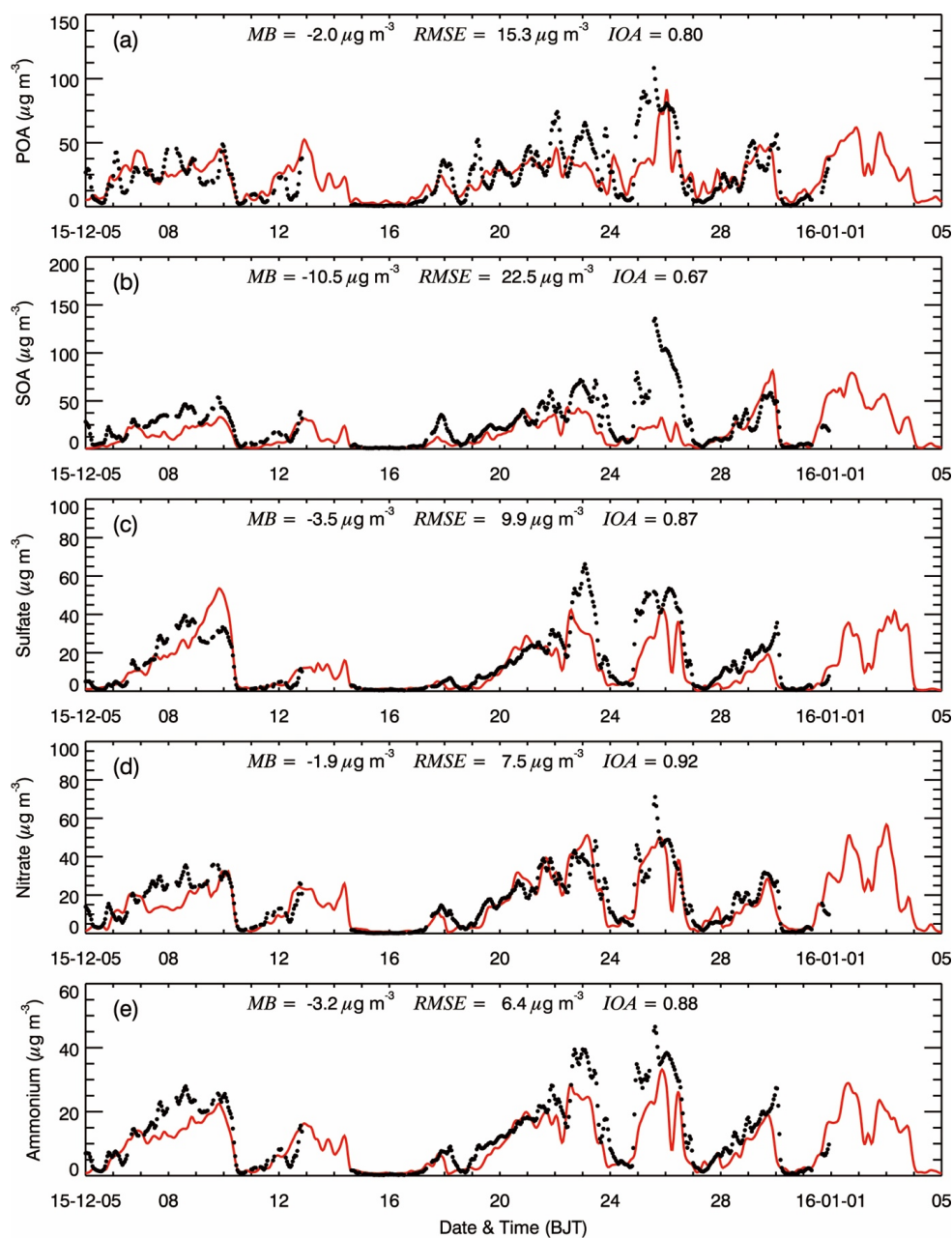Chemistry
and Physics
Discussions

Open Access

EGU
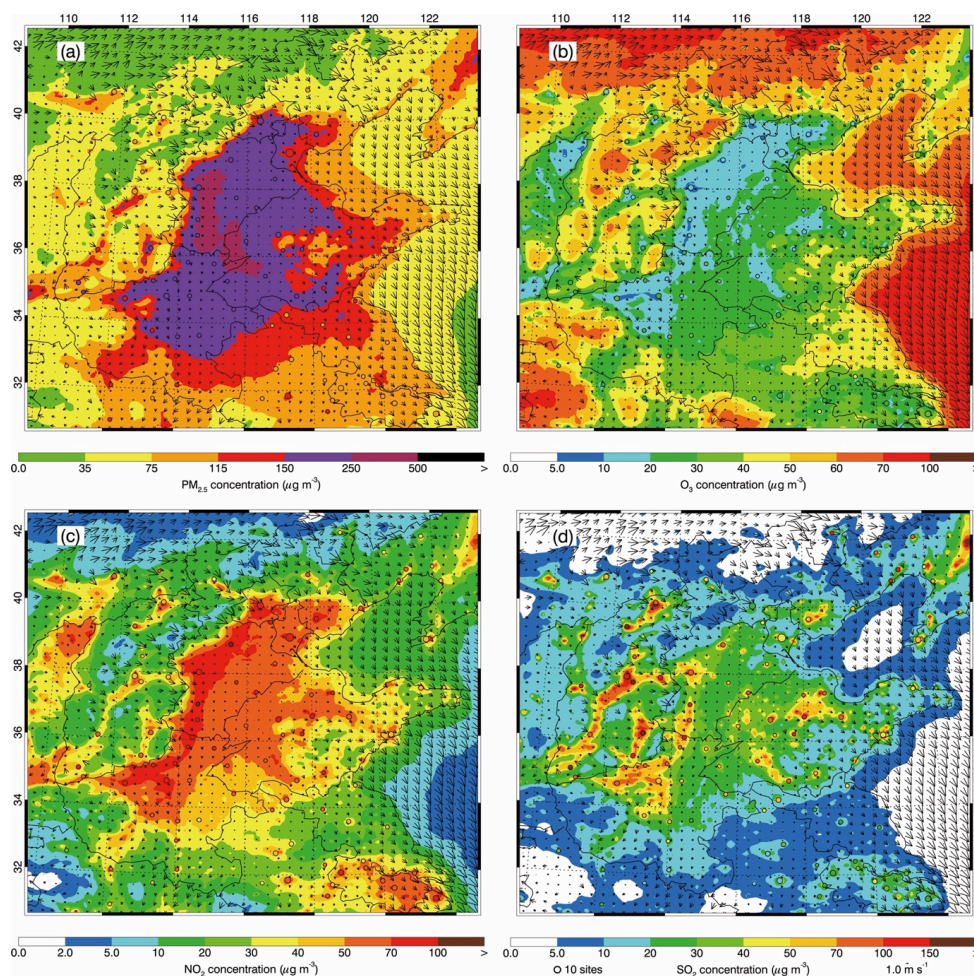


Figure 6 Pattern comparisons of simulated (color counters) vs. observed (colored circles) near-surface mass concentrations of (a) $PM_{2.5}$, (b) $O_3$, (c) $NO_2$, and (d) $SO_2$ averaged from 05 December 2015 to 04 January 2016. The black arrows indicate simulated surface winds.

892
893
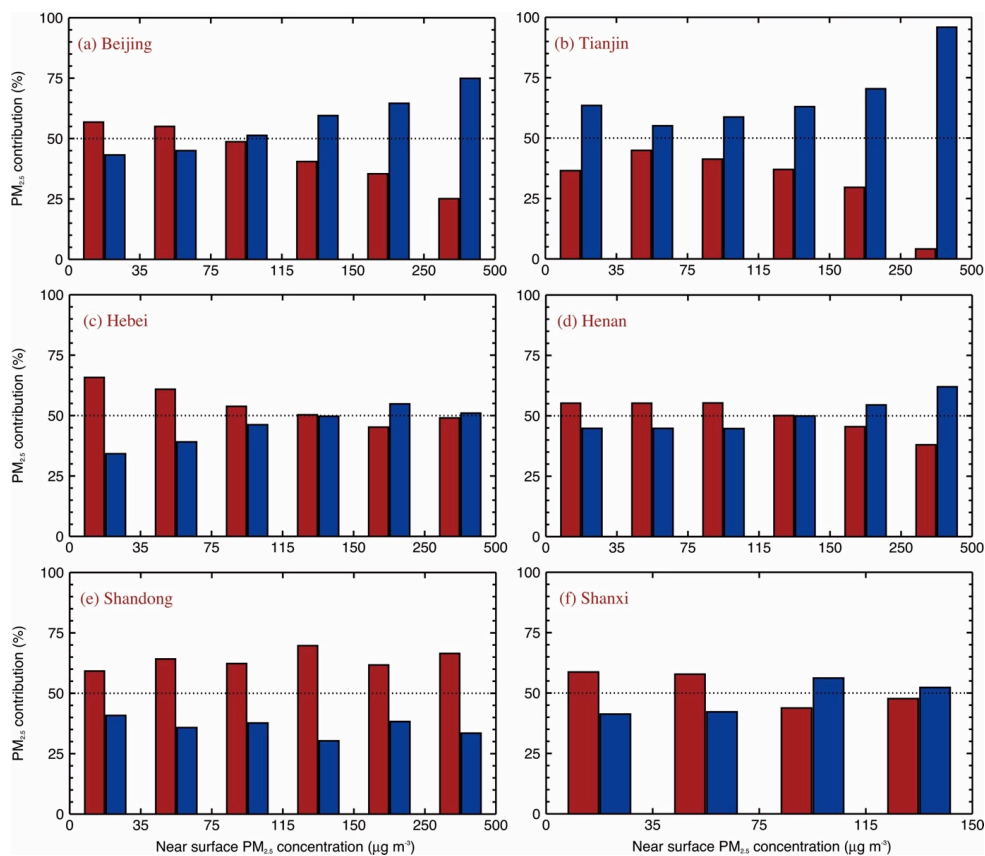894 Figure 7 Comparison of measured (black dots) and simulated (black line) diurnal profiles of
895 submicron aerosol species of (a) POA, (b) SOA, (c) sulfate, (d) nitrate, and (e) ammonium at
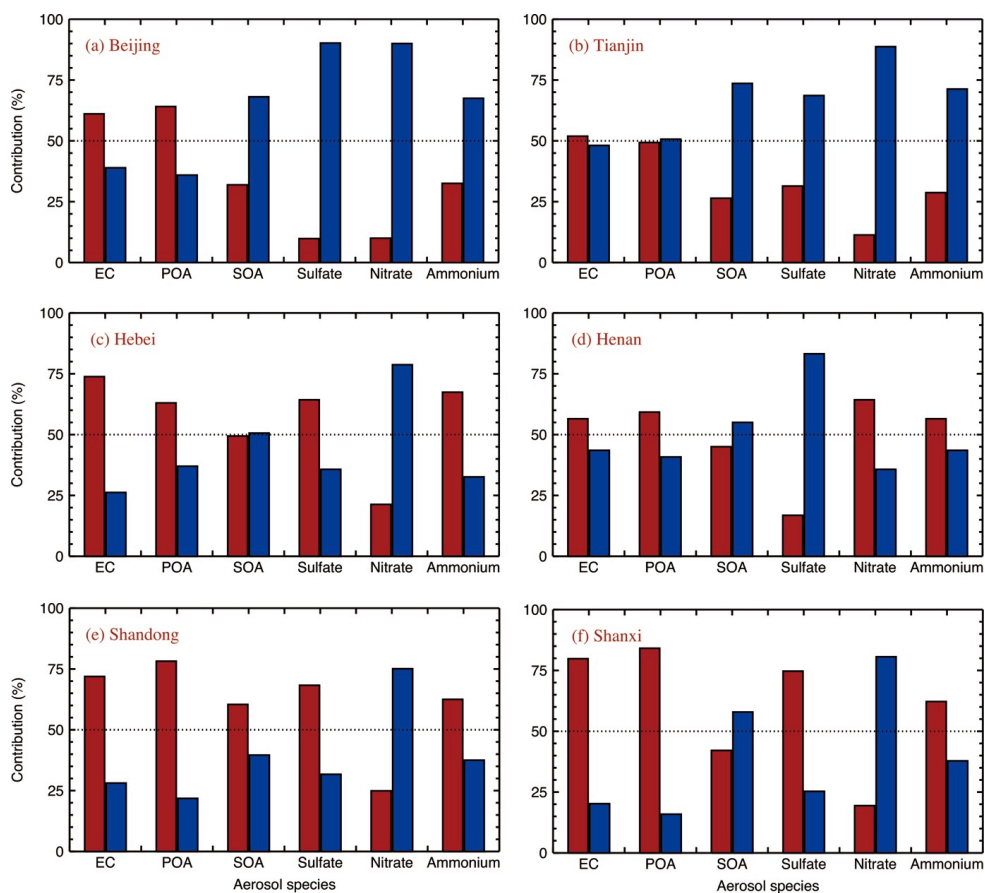896 NCNST site in Beijing from 05 December 2015 to 04 January 2016.
897
898
899
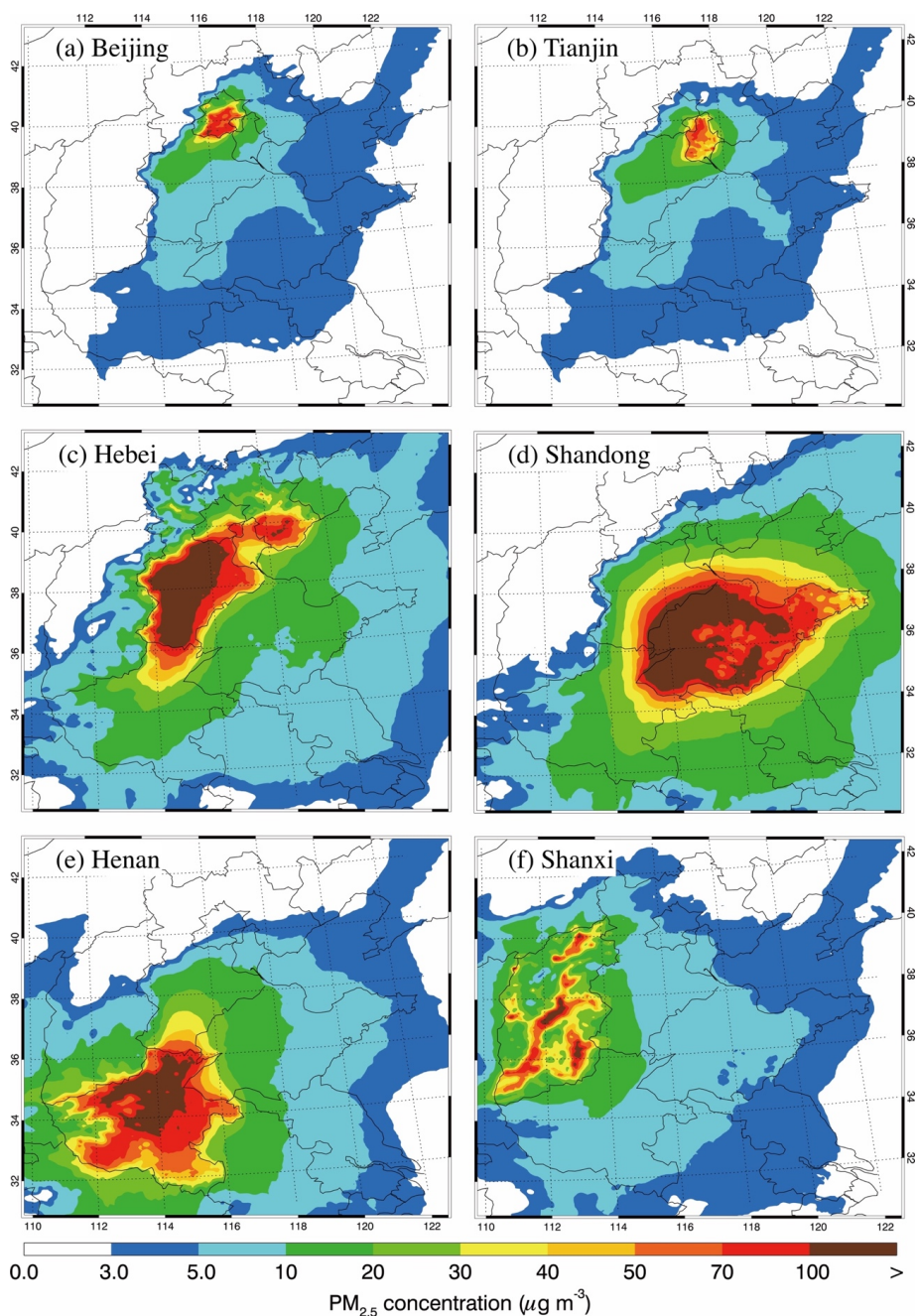
Figure 8 Spatial distribution of average PM$_{2.5}$ contributions from (a) Beijing, (b) Tianjin, (c) Hebei, (d) Shandong, (e) Henan, and (f) Shanxi provinces from 05 December 2015 to 04 January 2016.

Figure 9 Average PM$_{2.5}$ contributions (%) in (a) Beijing, (b) Tianjin, (c) Hebei, (d) Henan, (e) Shandong, and (f) Shanxi from local (red) and non-local (blue) emissions from 05 December 2015 to 04 January 2016 under different pollution levels.

Figure 10 Average aerosol constituent contributions (%) in (a) Beijing, (b) Tianjin, (c) Hebei, (d) Henan, (e) Shandong, and (f) Shanxi from local (red) and non-local (blue) emissions from 05 December 2015 to 04 January 2016.